Austral Summer Southern Africa Precipitation Extremes Forced by the El Niño-Southern Oscillation and the Subtropical Indian Ocean Dipole

Andrew Hoell[1]

NOAA/Earth System Research Laboratory Physical Sciences Division, Boulder, CO, USA

Linyin Cheng

NOAA/Earth System Research Laboratory Physical Sciences Division, Boulder, CO, USA

Cooperative Institute for Research in the Environmental Sciences

University of Colorado Boulder, Boulder, CO, USA

Submitted to *Climate Dynamics*, March 5, 2017

In Revision, *Climate Dynamics*, June 27, 2017

[1] Corresponding Author Address: Andrew Hoell, NOAA/Earth System Research Laboratory Physical Sciences Division, 325 Broadway, Boulder, CO 80305, email: andrew.hoell@noaa.gov

Abstract

Southern Africa, defined here as the African continent south of 15˚S latitude, is prone to seasonal precipitation extremes during December-March that have profound effects on large populations of people. The intensity of summertime precipitation extremes can be remarkable, with wet seasons experiencing up to a doubling of the seasonal average precipitation. Recognizing the importance of understanding the causes of Southern Africa precipitation extremes for the purpose of improved early warning, an 80-member ensemble of atmospheric model simulations forced by observed time-varying boundary conditions during 1979-2016 is used to examine the mechanisms by which December-March precipitation extremes are delivered to Southern Africa and whether the El Niño-Southern Oscillation (ENSO) and the Subtropical Indian Ocean Dipole (SIOD) modify the probabilities of extreme seasonal precipitation occurrences.

The model simulations reveal that the synchronous ENSO and SIOD phasing conditions the probability of December-March extreme precipitation occurrences. The probability of extreme wet seasons is greatly increased by La Niña, especially so when combined with a positive SIOD, and greatly decreased by El Niño regardless of SIOD phasing. By contrast, the probability of extreme dry seasons is increased by El Niño and is decreased by La Niña. The mechanisms by which extreme precipitation are delivered are the same regardless of ENSO and SIOD phase. Extreme wet seasons are a result of an anomalous lower tropospheric cyclone over Southern Africa that increases convergence and moisture fluxes into the region while extreme dry seasons are a result of an anomalous lower tropospheric anticyclone that decreases convergence and moisture fluxes into the region.

1. Introduction

During December-March, the climate of Southern Africa, defined here as the African Continent south of 15˚S, is sensitive to sea surface temperature (SST) anomaly patterns over the Pacific and Indian Oceans associated with the El Niño-Southern Oscillation (ENSO) and the Subtropical Indian Ocean Dipole (SIOD). The Austral summer climate over Southern Africa is especially sensitive to the synchronous behaviors of ENSO and SIOD (Hoell et al. 2016) as well as the individual effects of both ENSO (e.g. Nicholson and Entekhabi 1986, Lindesay 1988, Jury et al. 1994, Rocha and Simmonds 1997, Nicholson and Kim 1997, Reason et al. 2000, Misra 2003) and SIOD (Behera et al. 2000, Behera and Yamagata 2001, Reason 2001, Washington and Preston 2006, Manatsa 2015). Previous analyses have largely highlighted the most likely Southern Africa climate conditions related with ENSO and SIOD through averages of Southern Africa precipitation and the atmospheric circulation across many ENSO and SIOD events. In this analysis, we focus instead on December-March seasonal precipitation extremes over Southern Africa. We examine the mechanisms by which precipitation extremes are delivered to Southern Africa and whether synchronous ENSO and SIOD behaviors condition the occurrence probability of extreme wet and dry seasons.

December-March is the height of the Southern Africa rainy season and is the season in which Southern Africa is most closely related with ENSO (Manatsa 2015). The relationship between Southern Africa precipitation and ENSO provides opportunities for seasonal forecasting (Goddard and Dilley 2005) and has therefore supported the successful prediction of the region's precipitation during many Austral summers (e.g. Hastenrath et al. 1995). On average, December-March Southern Africa precipitation is below average during the positive phase of ENSO (El Niño) and is above average during the negative phase of ENSO (La Niña) (e.g.

Nicholson and Entekhabi 1986, Lindesay 1988, Jury et al. 1994, Rocha and Simmonds 1997, Nicholson and Kim 1997, Reason et al. 2000, Misra 2003, Manatsa 2015). La Niña is related to anomalous low pressure over Southern Africa, which in turn force anomalous upward motion and enhanced moisture fluxes into and over the region. El Niño is related to anomalous high pressure over Southern Africa, which in turn force anomalous downward motion and reduced moisture fluxes into and over the region (Ratnam et al. 2014, Hoell et al. 2015). SST anomaly patterns, however, differ from one El Niño event or La Niña event to the next (e.g. Wyrtki 1975, Capotondi et al. 2015). Recent research suggests that different SST anomaly patterns between ENSO events may have important effects on Southern Africa climate during Austral summer (Ratnam et al. 2014, Hoell et al. 2015). Another complicating factor in the Southern Africa response to ENSO is the effect of internal variability of the atmosphere. For example, during the 1997-1998 El Niño, the strength and position of the Angola low provided more precipitation than was expected over Southern Africa (Reason and Jagadheesha 2005, Lyon and Mason 2009).

Southern Africa precipitation during December-March is also related to a southwest-to-northeast oriented SST anomaly dipole over the western Indian Ocean associated with the SIOD phenomenon (e.g. Behera and Yamagata 2001, Reason 2001, Washington and Preston 2006, Hoell et al. 2016). The SST anomalies associated with the SIOD act to modify the flux of moisture and therefore precipitation over Southern Africa.

ENSO and SIOD synchrony affect Southern Africa beyond the individual effects of either ENSO or SIOD alone. Using a large ensemble of atmospheric model simulations, Hoell et al. (2016) found that when ENSO and SIOD are in opposite phases (e.g. El Niño and a negative SIOD or La Niña and a positive SIOD), the ENSO and SIOD responses are on average complimentary, and act to produce strong anomalous circulations, moisture fluxes and precipitation over Southern Africa. By contrast, when ENSO and SIOD are in the same phase (e.g. El Niño and a positive SIOD and La Niña and a negative SIOD), the ENSO and SIOD responses on average disrupt one another, and act to produce weaker anomalous circulations, moisture fluxes and precipitation over Southern Africa. Similar efforts by Manatsa et al. (2011, 2012) to decouple the effects of Indian and Pacific Ocean SST on Southern Africa climate using only observations were complicated by what appears to be changes in the behavior of the Southern Africa atmospheric circulation during the 1970s and 1990s. It is unclear whether the changes in the behavior of the atmospheric circulation that Manatsa et al. (2011, 2012) identified were a result of a forced oceanic response, internal atmospheric variability or a combination of the two.

The location of Southern Africa within the Southern Hemisphere subtropics shapes the region's semi-arid climate and therefore its propensity for December-March precipitation extremes (Mason and Jury 1997). On average during December-March, the St. Helene high is located to the west over the Atlantic Ocean and the Mascarene high is located to the east over the Indian Ocean (Fig. 1a). The eastern extent of the St. Helene high provides for anticyclonic circulation over Southern Africa and is therefore largely responsible for the region's semi-arid climate. Regionally, the Angola low serves as an important control on Southern Africa climate after its development during summer, by affecting the amount of moisture and movement of tropical-temperature troughs into the region (Kuhnel 1989; Todd and Washington 1999; Reason and Mulenga 1999; Jury 2013). The pathways for moisture transport are numerous over Southern Africa, coming from the Indian Ocean (D'Abreton and Lindesay 1993; D'Abreton and Tyson 1995, Rouault et al. 2003), the Atlantic Ocean and central-sub-Saharan Africa (Rouault et al. 2003; Cook et al. 2004).

Changes in the zonal extents of the St. Helene and Mascarene highs were responsible for the wettest and driest December-March seasons over Southern Africa during 1979-2016. During December-March 1999-2000, the wettest Southern Africa season in which twice the regional rainfall fell, the St. Helene high retreated to the west and the Mascarene high expanded to the west (Fig. 1b). The changes in the zonal extents of the subtropical high pressure areas resulted in anomalous cyclonic circulation regionally, an increased westward flux of moisture from the Indian Ocean and enhanced precipitation (Fig. 1d). During December-March 1982-1983, the driest Southern Africa season in which half of the regional rainfall fell, the St. Helene high strengthened greatly and expanded eastward (Fig. 1c). The changes in the zonal extents of the subtropical high pressure areas resulted in anomalous anticyclonic circulation regionally, a decreased flux of moisture from the Indian Ocean and reduced precipitation (Fig. 1e).

The wettest and driest December-March seasons during 1979-2016 both occurred during ENSO events: the wettest season of 1999-2000 during La Niña and the driest season of 1982-1983 during El Niño (Fig. 2). The Indian and Pacific Ocean SST anomalies during the wettest season of 1999-2000 were characterized by an anomalously cool tropical central and eastern Pacific Ocean and a warm-to-cold southwest-to-northeast dipole of SST over the southwest Indian Ocean (Fig. 2a). This Indian and Pacific Ocean SST pattern is related with an increased frequency of tropical cyclones affecting eastern portions of Southern Africa (Ash and Matyas 2012), as was the case during 1999-2000 when Cyclone Eline contributed immensely to seasonal rainfall over Mozambique. By contrast, the Indian and Pacific Ocean SST anomalies during the driest season of 1982-1983 were characterized by an anomalously warm tropical central and eastern Pacific Ocean and a cold-to-warm southwest-to-northeast dipole of SST over the southwest and central Indian Ocean (Fig. 2b).

While the wettest and driest December-March seasons during 1979-2016 occurred during ENSO events with dipole SST patterns in the western Indian Ocean characteristic of SIOD, limited evidence currently exists to suggest whether ENSO or SIOD condition the probability of seasonal precipitation extremes. The only work to address a similar question was by Washington and Preston (2006), whose study isolated only the Indian Ocean effects on extreme wet seasons.

In this manuscript, we examine the mechanisms by which December-March precipitation extremes are delivered to Southern Africa and whether the synchronous behavior of ENSO and the SIOD modify the probabilities of extreme wet and dry seasons. This work compliments studies such as Landman et al. (2005), which addressed prediction capabilities of seasonal precipitation extremes in past generations of global climate models, and Washington and Preston (2006), which isolated the Indian Ocean effects during extreme wet seasons. The nature and causes of Southern Africa precipitation extremes are examined using an 80-member ensemble of atmospheric model simulations forced by observed time-varying boundary conditions during 1979-2016. Wet and dry extremes are defined to occur when precipitation falls in the top and bottom 15%, respectively, of the 2960 December-March seasons generated from the large ensemble of atmospheric model simulations. Such an analysis would be impossible using observations alone due to the lack an adequately large sample size from which to identify extremes. In section 2, we describe the ensemble of atmospheric model simulations and the methodological approaches of the analyses. In section 3, we examine the mechanisms that deliver wet and dry precipitation extremes over Southern Africa and whether ENSO and SIOD modify the probability of extreme precipitation seasons. In section 4, we provide a summary.

2. Tools and Methods

2.1 Tools

2.1.1 Observations and Reanalyses

Observed precipitation on a 1.0˚x1.0˚ fixed grid is drawn from the Global Precipitation Climatology Centre (GPCC) version 7 (Schneider et al. 2013). Observed SSTs on a 1.0˚x1.0˚ fixed grid are drawn from the merged Hadley-NOAA Optimum Interpolation data set (Hurrell et al. 2008). Observed SST from Hurrell et al. (2008) are used to identify ENSO and SIOD events and to specify the ocean boundary conditions in the atmospheric model simulations. The observed atmospheric circulation on a 2.5˚x2.5˚ fixed grid is estimated using the NCEP-NCAR reanalysis I (Kalnay et al. 1996). A 1981-2010 mean is used to calculate anomalies of all variables.

2.1.2 Atmospheric Model Simulations

An ensemble of atmospheric model simulations forced by observed time-varying boundary conditions during 1979-2016 is utilized to assess Southern Africa precipitation extremes. The atmospheric model simulations are referred to as AMIP simulations after the Atmospheric Model Intercomparison Project (Gates 1992). All of the AMIP ensemble members are driven by identical observed monthly time-varying boundary conditions: SSTs, sea ice concentrations, greenhouse gases and ozone. The weather variability in each AMIP ensemble member is different since all of the simulations begin from different initial atmospheric states on 1 January 1978.

The ensemble of AMIP simulations consists of 80 members: 30 members are generated using the ECHAM5 atmospheric model (Roeckner et al. 2006) and 50 members are generated using the GFS model version 2 (Saha et al 2014). The ECHAM5 model is integrated on a T159 horizontal grid (~0.75˚x1.5˚ latitude-longitude) with 31 vertical levels. The GFS model is integrated on a T126 horizontal grid (~1˚x1˚ latitude-longitude) with 64 vertical levels. Outputs from the ECHAM5 and GFS models are interpolated to a common 1˚x1˚ fixed grid for analysis. Anomalies for each ensemble member are calculated relative to a 1981-2010 mean of that model. The ensemble of AMIP simulations is the same as in Hoell et al. (2016), except the AMIP ensemble used here is updated through March 2016. For more information and to obtain the AMIP simulations please visit the URL http://www.esrl.noaa.gov/psd/repository/alias/facts/.

We are of the opinion that for our purposes of this analysis that the benefits of using AMIP simulations outweigh the benefits provided by alternate methodologies, such as coupled climate model simulations. In terms of AMIP simulation drawbacks, Copsey et al. (2006) suggests that fixed SSTs in AMIP simulations may lead to a misrepresentation of sea level pressure over Southern Africa in response to Indian Ocean warming. Coupled climate model simulations, in which SSTs are not prescribed, but rather simulated through multi-way feedbacks across the climate system, serve as an alternative tool to AMIP simulations to assess Southern Africa climate. Problematically, there are biases in the SST anomaly patterns of ENSO simulated by coupled climate models (e.g. Captondi et al. 2006, Capotondi et al. 2010, Guilyardi et al. 2009, Yang and Giese 2013, Bellenger et al. 2014, Capotondi et al. 2015). Due to the SST biases in coupled climate model simulations, and to maintain continuity with the methodology of Hoell et al. (2016), we use AMIP simulations in this study.

Key to an analysis of December-March seasonal extremes in terrestrial Southern Africa precipitation is that both of the ECHAM5 and GFS models run in AMIP mode reproduce the similar precipitation characteristics as in observations. Spatially, the ECHAM5 and GFS AMIP simulations reproduce features of the observed Southern Africa precipitation during 1979-2016. The December-March average precipitation of the ECHAM5 and GFS models shares the same spatial patterns as the observed precipitation, though both models exhibit a dry bias over the rainiest parts of the region, which include Mozambique and Zimbabwe, and wet biases over Lesotho (Figs. 3a-c). Similarly, the December-March precipitation variance of the ECHAM5 and GFS models share the same spatial patterns as the observed precipitation, but the ECHAM5 model simulates slightly less variance over the rainiest parts of Southern Africa (Figs. 3d-f). Box and whisker plots of precipitation indicate that both the ECHAM5 and GFS models capture the seasonal cycle of the monthly precipitation central tendency (Fig. 4). We note, however, that the models exhibit greater precipitation spread during each month when compared with GPCC, likely due to the small sample size of observations relative to the sample size drawn from the ensemble of simulations.

Both the ECHAM5 and GFS models run in AMIP mode reproduce features of the observed areally averaged terrestrial Southern Africa precipitation south of 15˚S, thus supporting their use in the identification and examination of extremes in regional precipitation during December-March 1979-2016. The ECHAM5 and GFS models capture the homogeneous variation of Southern Africa precipitation with the areally averaged Southern Africa precipitation south of 15˚S when compared with observations (Figs. 5a-c). Furthermore, the shape of the ECHAM5 and GFS standardized precipitation anomaly PDFs are similar to the standardized observed precipitation PDF during December-March 1979-2016 (Fig. 5d). Standardized precipitation anomalies are analyzed due to the slight dry bias of the atmospheric models when compared with observations (Fig. 3), to maintain consistency with the analyses in Hoell et al. (2016) and to focus on the magnitude of precipitation anomalies for the assessment of extremes.

The atmospheric models run in AMIP mode capture key features of the observed temporal variability in areally averaged terrestrial Southern Africa precipitation south of 15˚S during December-March 1979-2016 (Fig. 6). Ensemble average precipitation of the AMIP simulations, which isolates the precipitation signal forced by the prescribed boundary conditions (e.g. SSTs), corresponds closely with the observed precipitation on interannual time scales during prolonged periods. This close correspondence reinforces the important relationship between the prescribed boundary conditions, and specifically the SSTs, and Southern Africa precipitation (Landman et al. 2014). Furthermore, the observed precipitation always falls within the ensemble spread of the AMIP simulations, which indicates that the models simulate realistic ranges of internal atmospheric variability in the presence of the observed boundary forcing.

2.2 Methods

2.2.1 Identification of ENSO and SIOD Events

ENSO and SIOD events are separated into five categories during December-March 1979-2016: (1) ENSO neutral, (2) El Niño and a negative SIOD (EN-SIOD), (3) El Niño and a positive SIOD (EN+SIOD), (4) La Niña and a negative SIOD (LN-SIOD) and (5) La Niña and a positive SIOD (LN+SIOD). The seasonal occurrences of each ENSO and SIOD category are shown in Table 1. ENSO events are identified based upon a threshold exceedance of the Niño3.4 index anomaly relative to a 1981-2010 baseline during December-March. The Niño3.4 index is defined as the areally averaged SSTs over the region 5˚S-5˚N, 170˚W-120˚W. El Niño is defined to occur when the Niño3.4 index anomaly exceeds 0.5˚C and La Niña is defined to occur when the Niño3.4 index anomaly falls below -0.5˚C. ENSO neutral is defined to occur when the Niño3.4 index falls between -0.5˚C and 0.5˚C. The sign of the SIOD anomaly is identified using the SIOD index of Behera and Yamagata (2001) during December-March. Behera and Yamagata (2001) define the SIOD as the areally average SST anomaly over 28˚S-18˚N, 90˚E-100˚E subtracted from areally average SST anomaly over 37˚S-27˚S, 55˚E-65˚E.

The SST anomaly patterns of four December-March 1979-2016 ENSO and SIOD categories are shown in Fig. 7. EN-SIOD is distinguished by warm SST anomalies in the central and eastern Pacific Ocean that define El Niño and a southwest to northeast oriented dipole of SSTs over the Indian Ocean that define a negative phase of the SIOD (Fig. 7a). EN+SIOD is distinguished by warm SST anomalies in the central Pacific Ocean that define El Niño, but lacks the southwest to northeast oriented dipole of SSTs over the Indian Ocean that define the SIOD (Fig. 7a). LN-SIOD is distinguished by cold SST anomalies in the central and eastern Pacific Ocean that define La Niña, but lacks the southwest to northeast oriented dipole of SSTs over the Indian Ocean that define the SIOD (Fig. 7a). LN+SIOD is distinguished by cold SST anomalies over the central and eastern Pacific Ocean that define La Niña and a southwest to northeast oriented dipole of SSTs over the Indian Ocean that define a positive phase of the SIOD (Fig. 7d).

Since the SST anomalies characteristic of both ENSO and SIOD rely on atmosphere-ocean coupling in their lifecycles, there is a question as to whether SST anomalies over the Pacific associated with ENSO may in turn force an atmospheric teleconnection that at least partially drives SST anomalies that define the SIOD. Such a notion calls into question the independence of the SIOD from ENSO. Current evidence suggests that ENSO is not linearly related with Indian Ocean SSTs that define the SIOD (Wang 2010), though at this time it cannot be ruled out that some nonlinear relationships may exists. Wang (2010) argues that the forcing of the SIOD is a result of the ocean mixed layer response to changes in the subtropical high pressure areas, which modifies the latent heat flux due to evaporation.

It is important to note that differences in the Southern Africa precipitation responses can arise due to the differences between the SST anomaly pattern of each season that falls into an ENSO and SIOD phase combination and the average of each ENSO and SIOD phase combination. Differences in SST patterns and therefore the Southern Africa precipitation response can arise over the Pacific Ocean due to different ENSO flavors (e.g. Ratnam et al. 2014 and Hoell et al. 2015) the Indian Ocean (e.g. Reason 2001 and Washington and Preston 2006) and the Atlantic Ocean (e.g. Reason 1998, 1999).

2.2.2 Identification of Southern Africa Precipitation Extremes

The size of a single observed 37-year time series renders it inadequate to identify and examine seasonal December-March Southern Africa precipitation extremes, and how ENSO and SIOD phase combinations condition those extremes. We therefore utilize the 80-member AMIP ensemble during 1979-2016, which provides a sample size of 2960 December-March seasons, to analyze the nature and causes of precipitation extremes. It is our goal that the 80-member ensemble of atmospheric model simulations will compensate for the small number of unique ENSO and SIOD phase combinations during 1979-2016. The large ensemble of atmospheric model simulations allows for sample sizes of 640, 320, 480 and 560 in the EN-SIOD, EN+SIOD, LN+SIOD and LN-SIOD phase combinations, respectively. These are noteworthy sample sizes, from which we believe that we can adequately assess the sensitivity of Southern Africa precipitation extremes to ENSO and SIOD phase combinations.

December-March Southern Africa precipitation extremes are identified through a threshold exceedance of areally averaged terrestrial Africa precipitation south of 15˚S (Fig. 6). Extreme wet seasons are defined to occur when simulated Southern Africa precipitation falls within the top 15% of the sample. Extreme dry seasons are defined to occur when simulated Southern Africa precipitation falls within the bottom 15% of the sample. The 15% thresholds correspond to 0.53 and -0.53 standardized departures, respectively (Fig. 6, dashed horizontal lines), which isolates 444 extreme wet and dry seasons.

2.2.3 Assessment of Extreme Wet and Dry Occurrences During ENSO and SIOD Phases

Two approaches are used to assess the likelihood of extreme wet and dry Southern Africa December-March seasons as a function of ENSO and SIOD phase combinations in the 80-member AMIP ensemble. The first approach estimates the frequency of extreme Southern Africa precipitation occurrences per 37 December-March seasons, where 37 corresponds to the number of seasons during 1979-2016. 37 random Southern Africa precipitation samples are selected during each ENSO and SIOD phase combination, and the number of samples that exceed or fall below the wet and dry extreme thresholds are counted. This process is repeated 10,000 times to construct a distribution of Southern Africa wet and dry extreme occurrences per 37 years for each ENSO and SIOD phase combination.

The second approach estimates the return period for distinct precipitation thresholds during ENSO and SIOD phase combinations. The return period is estimated through an application of the Generalized Pareto Distribution (GPD), known as the peak-over-threshold approach, and is derived based on exceedances above a certain threshold. GPD has three distribution parameters: the scale parameter σ_u quantifies the spread (or variance) of the GPD and the shape parameter ξ describes whether the tail is bounded ($\xi < 0$), light ($\xi \rightarrow 0$) or heavy ($\xi > 0$) (Coles et al. 2001; De Haan and Ferreira 2007). Thresholds are chosen at a level where the data above it approximately follows a GPD. The shape and scale parameters are estimated at a high threshold (Dupuis 1999; Davison and Smith 1990). Different quantiles of precipitation corresponding to each scenario, e.g. 0.75, 0.80, and 0.85 are tested as the threshold u herein.

The goodness-of-fit of the model is assessed using a graphical diagnostic method known as Quantile-Quantile (Q-Q) plots. Q-Q plots compare the modeled GPD distribution and empirical probability distribution by plotting their quantiles against each other. This examination confirms that GPD is a good fit to the exceedances of the AMIP simulations for the top 15% of the precipitation distribution (e.g. 85% quantile). We therefore select exceedance beyond the 85% quantile as the threshold, which can help to inform more severe rainfall events (not shown for brevity).

Uncertainty is assessed using a Bayesian-based Markov chain approach that is integrated into the GPD (Coles and Pericchi 2003; Parent and Bernier 2003; Coles and Powell 1996). This approach combines the knowledge brought by a prior distribution of parameters and the observed vector of exceedances $\vec{y} = (y_i)_{i=1:N_t}, \text{i.e.}\, y_i > u,$ into the posterior distribution of GPD parameters. The inferred distribution parameters, i.e. $\theta = (\sigma_u, \xi)$ are then be used to estimate the return level vs. return period of extreme precipitation for each scenario as follows:

$$T_y = u + \frac{\sigma_u}{\xi} \times [(\frac{n_y}{1-P} \times \zeta_u)^{\xi} -1] \quad (1)$$

where p is the non-exceedance probability of occurrence; T_y is the T-year precipitation return level, referring to the extreme rainfall of specified intensity having a probability of exceedance of $\frac{1}{T}$ and $T = \frac{1}{1-P}$, i.e. the average length of time between events of a given intensity; n_y represent the number of observations taken in a year, and ζ_u describes the probability of exceedances, i.e., $\zeta_u = p(y_i > u)$. We show the upper (97.5th percentile) and lower credible intervals (2.5th percentile) of the 15- to 200-yr return levels for the standardized precipitation in each scenario to inform the associated uncertainty. In this study, the Bayesian analysis of return level and return period based on the GPD approach designed for risk analysis of hydrologic and climatic extremes (see Cheng et al. 2014).

2.2.4 Statistical Significance Assessment of Spatial Anomaly Composites

A resampling approach is used to assess statistical significance at each grid cell of spatial anomaly composites. Random samples of each variable are selected without replacement from the entire population of data, where the number of randomly selected samples correspond to the sample size used to construct the corresponding anomaly composite. The random samples are averaged and the processes is repeated 10,000 times to construct a distribution. The statistical significance at $p<0.025$ for each tail is assessed from the 10,000-member distribution.

3. Results

3.1 Most Common Mechanisms Associated with Southern Africa Precipitation Extremes

Wet precipitation extremes over Southern Africa during December-March are on average related with Indo-Pacific SST anomalies characteristic of LN+SIOD (c.f. Fig. 8b and Fig. 7d) and anomalous atmospheric circulations that bear close resemblance to the LN+SIOD atmospheric response (c.f. Fig. 8a and Figs. 9 and 10 in Hoell et al. 2016). The average Indo-Pacific SST anomalies during wet Southern Africa precipitation extremes are characterized by a warm-to-cool southwest-to-northeast SST anomaly dipole over the Indian Ocean that defines a positive phase of the SIOD and cool tropical central and eastern Pacific Ocean SST anomalies that define La Niña. Regionally, the average anomalous atmospheric circulation during wet Southern Africa precipitation extremes bears close resemblance to conditions during the observed extreme wet season of 1999-2000 (c.f. Fig. 8a and Figs. 1d), as evidenced by an anomalous lower tropospheric cyclone, which produces tropospheric convergence, and an enhanced flux of moisture into the region that results in enhanced precipitation. Globally, wet Southern Africa precipitation extremes are related with strong anomalous convergence over the eastern Indian Ocean and the Maritime Continent and strong anomalous divergence over the central Indian Ocean that flows into the anomalous cyclone positioned over Southern Africa.

Dry precipitation extremes over Southern Africa during December-March are on average related to SSTs and anomalous atmospheric circulations that are nearly equal and opposite to those of wet extremes (Fig. 8). Dry precipitation extremes over Southern Africa during December-March are on average related with Indo-Pacific SST anomalies characteristic of EN-SIOD (c.f. Fig. 8d and Fig. 7a) and anomalous atmospheric circulations that bear close resemblance to the EN-SIOD atmospheric response (c.f. Fig. 8c and Figs. 9 and 10 in Hoell et al. 2016). The average Indo-Pacific SST anomalies during dry Southern Africa precipitation extremes are characterized by a cold-to-warm southwest-to-northeast SST anomaly dipole over the Indian Ocean that defines a negative phase of the SIOD and warm tropical central and eastern Pacific Ocean SST anomalies that define El Niño. Regionally, the average anomalous atmospheric circulation during dry Southern Africa precipitation extremes bears close resemblance to conditions during the observed extreme dry season of 1982-1983 (c.f. Fig. 8c and Figs. 1e), as evidenced by an anomalous lower tropospheric anticyclone, which produces tropospheric divergence, and a reduced flux of moisture into the region that results in suppressed precipitation. Globally, dry Southern Africa precipitation extremes are related to anomalous divergence over the eastern Indian Ocean and the Maritime Continent and anomalous divergence over the central Indian Ocean which helps to draw atmospheric mass away from Southern Africa.

3.2 Southern Africa Precipitation Extremes Conditioned by ENSO and SIOD

Here we quantify how ENSO neutral and the four ENSO and SIOD phase combinations condition the probability of wet and dry Southern Africa precipitation extremes during December-March. La Niña doubles the frequency of wet Southern Africa precipitation extremes relative to ENSO neutral while El Niño halves the frequency of wet Southern Africa precipitation extremes relative to ENSO neutral (Fig. 9a,b). SIOD further conditions the probability of wet extremes during La Niña, with extremes occurring more frequently during LN+SIOD than LN-SIOD. SIOD, however, has little effect on the probability of wet extremes during El Niño. For every 37 December-March ENSO neutral seasons, four of those seasons are most likely to experience wet extremes (Fig. 9a, black line). The spread in the distributions of wet precipitation extreme occurrences during ENSO neutral, and during all ENSO and SIOD phase combinations, highlights important effects of internal climate variabilities on seasonal extremes. ENSO neutral exerts a 25% chance of fewer than 2.5 extremes and a 25% chance of greater than 5.5 extremes for every 37 years (Fig. 9b, black line). La Niña effects a positive shift in the distributions of wet extremes relative to ENSO neutral, and SIOD exerts an important modifying effect on the frequency of the La Niña-related wet extremes. The modal value of wet extremes is 10 for every 37 LN+SIOD seasons (Fig. 9a, blue line) and 8.5 for every 37 LN-SIOD seasons (Fig. 9a, green line). Both LN+SIOD and LN-SIOD are related with larger spreads of wet precipitation extreme occurrences than during ENSO neutral (Fig. 9). This increased spread is demonstrated by a 25% chance of fewer than 8 extremes and a 25% chance of greater than 12 extremes during LN+SIOD (Fig. 9b, blue line) and a 25% chance of fewer than 6 extremes and a 25% chance of greater than 10 extremes during LN-SIOD (Fig. 9b, green line). By contrast, El Niño effects a negative shift in the distributions of wet extremes relative to ENSO neutral. SIOD has no effect on wet precipitation extremes during El Niño, as evidenced by nearly indistinguishable distribution functions of wet extremes during EN-SIOD and EN+SIOD (Figs. 9a,b, red and orange lines). Both EN-SIOD and EN+SIOD are related with a modal value of 2 wet extremes for every 37 years, with a 25% chance of fewer than 1.5 extremes and a 25% chance of greater than 3.5 extremes.

El Niño increases the frequency of dry Southern Africa precipitation extremes while La Niña decreases the frequency of wet Southern Africa precipitation extremes relative to ENSO neutral (Fig. 9c,d). SIOD further conditions the probability of dry extremes during both El Niño and La Niña: the frequency of dry extremes is increased during EN-SIOD relative to EN+SIOD and the frequency of dry extremes is decreased during LN+SIOD relative to LN-SIOD. For every 37 December-March ENSO neutral seasons, five of those seasons are most likely to experience dry extremes (Fig. 9c, black line). Again, we emphasize that the spread in the distribution of dry precipitation extreme occurrences during ENSO neutral and all ENSO and SIOD phase combinations demonstrates important effects of internal climate variabilities on seasonal extremes. ENSO neutral exerts a 25% chance of fewer than 3.5 extremes and a 25% chance of greater than 6 extremes for every 37 years (Fig. 9d, black line). El Niño effects a positive shift to the distribution of dry extremes relative to ENSO neutral, and SIOD in concert with El Niño further exerts an important modifying effect on the frequency of dry extremes. The modal value of dry extremes is 8 for every 37 EN-SIOD seasons (Fig. 9c red line) and 6.5 for every 37 EN+SIOD seasons (Fig. 9c, orange line). Both EN-SIOD and EN+SIOD are related with larger spreads in the distribution of dry precipitation extreme occurrences than during ENSO neutral (Fig. 9c). This increased spread is demonstrated by a 25% chance of fewer than 6.5 extremes and a 25% chance of greater than 9.5 extremes during EN-SIOD (Fig. 9d, red line) whereas EN+SIOD is associated with a 25% chance of fewer than 5 extremes and a 25% chance of greater than 8.5 extremes (Fig. 9d, orange line). By contrast, La Niña effects a negative shift of the distribution of dry extremes relative to ENSO neutral. During LN+SIOD, the modal value of dry extremes is 3.5 occurrences per 37 years (Fig. 9c, blue) while during LN-SIOD, the modal value of dry extremes is 4.5 (Fig. 9c, green line). LN+SIOD is associated with a 25% chance of fewer than 2 extremes and a 25% chance of greater than 5 extremes whereas (Fig. 9d, blue line) LN-SIOD is associated with a 25% chance of fewer than 2.5 extremes and a 25% chance of greater than 5.5 extremes (Fig. 9d, green line).

The return periods for discrete values of Southern Africa precipitation shown in Fig. 10 further demonstrates that La Niña provides a strong conditioning of heavy rainfall statistics relative to ENSO neutral and El Niño during December-March. The conditioning of heavy rainfall statistics during La Niña is additionally affected by SIOD phase. The strongest conditioning of heavy rainfall statistics occurs during LN+SIOD, where for all return periods the median precipitation amount associated with extreme events is about 45% greater than during ENSO neutral (Fig. 10a). A seasonal standardized precipitation departure of 1.5 occurs about every 30 years under LN+SIOD, whereas the same precipitation departure occurs about every 170 years under ENSO neutral. The non-overlapping estimations between the 95% significance level of LN+SIOD and the median of ENSO neutral indicate that the production of wet extremes during ENSO neutral as severe as during LN+SIOD is very unlikely at the 95% significance level (Fig. 10a). LN-SIOD also conditions the occurrence of heavy precipitation relative to

ENSO neutral, though not to the same degree as LN+SIOD (c.f. Figs. 10a and 10b). Heavy rainfall events in the 20 to 150-year return period range are reduced by 0.2 standardized departures during LN-SIOD than during LN+SIOD. However, the difference in the magnitude of precipitation extremes between LN-SIOD and LN+SIOD is not appreciable for return periods of greater than 150 years, though higher confidence is associated with LN+SIOD conditions, as evidenced by the spreads of the 95% uncertainty levels, which induce less uncertainty in the estimations of wet extremes.

El Niño strongly reduces the precipitation anomalies for discrete return periods relative to ENSO neutral and La Niña (Fig. 11). A seasonal standardized precipitation departure of 1.0 is a comparatively rare occurrence during El Niño, occurring only about once every 90 years during EN-SIOD and about once every 70 years during EN+SIOD. By contrast, the same seasonal standardized departure of 1.0 occurs about once every 25 years during ENSO neutral and more frequently than once every 20 years during both LN+SIOD and LN-SIOD. Furthermore, the non-overlapping estimations between the 95% significance level of EN-SIOD and the median of ENSO neutral indicate that the production of wet extremes during EN-SIOD as severe as during ENSO neutral is impossible at the 95% significance level (Fig. 11a).

A better appreciation for how ENSO and SIOD condition the probability of extreme December-March precipitation seasons is gained through examinations of the Southern Africa precipitation characteristics under ENSO neutral and ENSO and SIOD conditions. The distribution of Southern Africa precipitation during ENSO neutral is broad, which highlights the important effects of internal climate variabilities (Fig. 12a, black line). These internal variabilities are a result of the different boundary conditions specified during each ENSO neutral season (e.g. SSTs) and random variability of the atmospheric circulation. Southern Africa precipitation during ENSO neutral has little skew toward wet or dry conditions, as evidenced by a comparable mean and mode of the distribution (Table 2). The dry mode of the distribution and little skew leads to a slightly heavier dry tail to the ENSO neutral distribution, with 18% probability of exceeding the dry threshold and a 10% probability of exceeding the wet threshold (Fig. 12b, black line).

La Niña shifts the Southern Africa precipitation distribution to wet conditions and also widens the precipitation distribution relative to ENSO neutral (Fig. 12 and Table 2). The precipitation distribution widens during La Niña due to a heavy wet tail, with little change in the dry tail relative to ENSO neutral (Fig. 12a). SIOD introduces an important modifying effect on the Southern Africa precipitation during La Niña. There is little difference in the dry tails between LN+SIOD and LN-SIOD, with the probability of a dry occurrence residing around 12% for both phase combinations (Fig. 12b). However, LN+SIOD increases the wet tail of the distribution beyond LN-SIOD, with the probability of extreme wet occurrences residing around 30% for LN+SIOD relative to 20% for LN-SIOD (Fig. 12b).

El Niño shifts the Southern Africa precipitation distribution to dry conditions and narrows the precipitation distribution relative to ENSO neutral (Fig. 13 and Table 2). The precipitation distribution narrows slightly during El Niño due to an overall shift in the distribution to dry conditions except for the far dry tail (<-1.25 standardized departures). Unlike La Niña, the SIOD introduces a minor effect on Southern Africa precipitation during El Niño, as evidenced by nearly indistinguishable EN-SIOD and EN+SIOD distributions.

3.3. Mechanisms of Uncommon Southern Africa Precipitation Extremes

We previously showed that it is uncommon, though not impossible, for El Niño and ENSO neutral to force wet Southern Africa precipitation extremes and for La Niña and ENSO neutral to force dry Southern Africa precipitation extremes (Figs. 9-11). Interestingly, Southern Africa wet extremes during ENSO neutral and El Niño are forced regionally by the same mechanisms as the average of all extreme wet seasons (e.g. a La Niña-like response; c.f. Figs. 14a,c and Fig. 8a) and Southern Africa dry extremes during ENSO neutral and La Niña are forced regionally by the same mechanisms as the average of all extreme dry seasons (e.g. an El Niño-like response; c.f. Figs. 15a,c and Fig. 8c). Wet Southern Africa extremes during ENSO neutral and El Niño are forced by a lower tropospheric cyclone that results in tropospheric convergence and an enhanced flux of moisture into the region. Dry Southern Africa extremes during ENSO neutral and La Niña are forced by a lower tropospheric anticyclone that results in tropospheric divergence and a reduced flux of moisture into the region. The fact that low probability seasonal Southern Africa precipitation extremes can happen in the large ensemble of AMIP simulations thereby leads us to conclude that internal atmospheric variability local to the Southern Africa region can force extreme precipitation.

4. Summary

Southern Africa precipitation extremes during the December-March rainy season trigger the loss of life, damage of property and provoke lasting detrimental effects on ecosystems. Extreme dry conditions during 2014-2015 and 2015-2016 resulted in crop failures, food shortages and economic crises (The Guardian 2016; Al Jazeera 2016). Extreme wet conditions during the following season of 2016-2017 resulted in flooding, crop destruction and the displacement of people from their homes (IFRC 2017). In light of the exceptional societal effects of dry and wet extremes on Southern Africa, we sought to better understand the mechanisms by which these extremes are delivered to the region and how the region's two main climate drivers, ENSO and the SIOD, modify the probabilities of extreme December-March precipitation occurrences using an 80-member AMIP ensemble during 1979-2016. A better understanding of how ENSO and SIOD modify the probabilities of extreme Southern Africa precipitation occurrences may provide important early warning prior to the December-March rainy season.

The AMIP simulations suggest that the frequency of wet December-March Southern Africa extremes is doubled by La Niña and is halved by El Niño relative to ENSO neutral. The frequency of wet extremes during La Niña are further modified by SIOD phase, as wet extremes occur more frequently during LN+SIOD than LN-SIOD. LN+SIOD therefore conditions the strongest heavy rainfall statistics, where for all return periods the median precipitation amount associated with extreme events is about 45% greater than during ENSO neutral. Furthermore, a seasonal standardized precipitation departure of 1.5 occurs about every 30 years under LN+SIOD, whereas the same precipitation departure occurs about every 170 years under ENSO neutral. By contrast, El Niño strongly reduces the precipitation anomalies for discrete return periods relative to ENSO neutral and La Niña. Standardized precipitation departures of 1.0 or greater are comparatively rare occurrences during El Niño whereas they are quite common during ENSO neutral and La Niña.

The AMIP simulations also suggest that the frequency of dry December-March Southern Africa extremes is increased by 1.5 times by El Niño and is reduced by 1.5 times by La Niña when compared with ENSO neutral. SIOD further conditions the probability of dry extremes during both El Niño and La Niña: the frequency of dry extremes is increased during EN-SIOD relative to EN+SIOD and the frequency of dry extremes is decreased during LN+SIOD relative to LN-SIOD.

Wet and dry Southern Africa precipitation extremes are delivered by the same regional mechanisms regardless of ENSO and SIOD phase. Southern Africa wet extremes are caused by an anomalous lower tropospheric cyclone, which produces anomalous tropospheric convergence, and an enhanced flux of moisture into the region that results in enhanced precipitation, similar to the observed extreme wet season of 1999-2000. Southern Africa dry extremes are caused by an anomalous lower tropospheric anticyclone, which produces anomalous tropospheric divergence, and a reduced flux of moisture into the region that results in suppressed precipitation, similar to the observed extreme wet season of 1982-1983.

Knowledge of the state of ENSO has long been used to predict summertime Southern Africa precipitation (e.g. Hastenrath et al. 1995) since Nicholson and Entekhabi (1986) and Ropelewski and Halpert (1987) first identified the relationship between ENSO and Southern Africa climate. Our understanding of the important drivers of Southern Africa climate has since expanded to include the effects of the Indian Ocean as a result of the SIOD (e.g. Behera et al. 2000, Behera and Yamagata 2001, Reason 2001, Washington and Preston 2006, Manatsa 2015, Hoell et al. 2016). Parallel to the incremental advancements in our understanding of the drivers of Southern Africa climate, improvements in dynamical models have enhanced the predictability of Southern Africa precipitation (e.g. Yuan et al. 2014). These dynamical models, with ever-increasing ability to forecast SSTs (e.g Wang et al. 2009), utilize information of the ENSO and SIOD situations to produce seasonal Southern Africa forecasts.

Forecast models, however, are not yet perfect, and studies such as this provide valuable physical contexts to forecasters of Southern Africa climate. Specifically, how should forecasters interpret model projections of December-March climate based upon knowledge of the ENSO and SIOD states? Hoell et al. (2016) provided such context over Southern Africa, and showed how simultaneous ENSO and SIOD phasing produce complimentary or destructive atmospheric responses. In this paper, we provide further context on how ENSO and SIOD phasing condition the probability of Southern Africa precipitation extremes. Knowledge of precipitation extreme probabilities provides more information than simply the most likely seasonal average precipitation alone, especially so over regions like Southern Africa whose populations are already especially vulnerable to extreme climate conditions. Empowering forecasters with information on how ENSO and SIOD condition the probability of extreme precipitation occurrences allows them to provide critical early warning information on floods and droughts to mitigate the loss of life and property.

Acknowledgements

The authors thank Dave Allured for completing the ECHAM5 simulations and Tao Zhang for completing the GFS simulations. The authors also thank Judith Perlwitz and Marty Hoerling for thought-provoking discussions during the preparation of this manuscript. The authors are grateful for support from the Famine Early Warning Systems Network.

References

Ash, K. D., and C. J. Matyas, 2012: The influences of ENSO and the subtropical Indian Ocean Dipole on tropical cyclone trajectories in the southwestern Indian Ocean. International Journal of Climatology, 32, 41-56.

Behera, S. K., P. S. Salvekar, and T. Yamagata, 2000: Simulation of Interannual SST Variability in the Tropical Indian Ocean. Journal of Climate, 13, 3487-3499.

Behera, S. K., and T. Yamagata, 2001: Subtropical SST dipole events in the southern Indian Ocean. Geophysical Research Letters, 28, 327-330.

Bellenger, H., E. Guilyardi, J. Leloup, M. Lengaigne, and J. Vialard, 2014: ENSO representation in climate models: from CMIP3 to CMIP5. Clim Dyn, 42, 1999-2018.

Capotondi, A., 2013: El Niño–Southern Oscillation Ocean Dynamics: Simulation by Coupled General Circulation Models. Climate Dynamics: Why Does Climate Vary?, American Geophysical Union, 105-122.

Capotondi, A., A. Wittenberg, and S. Masina, 2006: Spatial and temporal structure of Tropical Pacific interannual variability in 20th century coupled simulations. Ocean Modelling, 15, 274-298.

Capotondi, A., and Coauthors, 2014: Understanding ENSO Diversity. Bulletin of the American Meteorological Society, 96, 921-938.

——, 2014: Understanding ENSO Diversity. Bulletin of the American Meteorological Society, 96, 921-938.

Cheng, L., A. AghaKouchak, E. Gilleland, and R. W. Katz, 2014: Non-stationary extreme value analysis in a changing climate. Climatic Change, 127, 353-369.

Coles, S., J. Bawa, L. Trenner, and P. Dorazio, 2001: An introduction to statistical modeling of extreme values. Vol. 208, London, Springer.

Coles, S., and L. Pericchi, 2003: Anticipating catastrophes through extreme value modelling. Journal of the Royal Statistical Society: Series C (Applied Statistics), 52, 405-416.

Coles, S. G., and E. A. Powell, 1996: Bayesian Methods in Extreme Value Modelling: A Review and New Developments. International Statistical Review / Revue Internationale de Statistique, 64, 119-136.

Cook, K. H., J. S. Hsieh, and S. M. Hagos, 2004: The Africa–South America Intercontinental Teleconnection. Journal of Climate, 17, 2851-2865.

Copsey, D., R. Sutton, and J. R. Knight, 2006: Recent trends in sea level pressure in the Indian Ocean region. Geophysical Research Letters, 33, n/a-n/a.

D'Abreton, P. C., and J. A. Lindesay, 1993: Water vapour transport over Southern Africa during wet and dry early and late summer months. International Journal of Climatology, 13, 151-170.

D'Abreton, P. C., and P. D. Tyson, 1995: Divergent and non-divergent water vapour transport over southern Africa during wet and dry conditions. Meteorol. Atmos. Phys., 55, 47-59.

Davison, A. C., and R. L. Smith, 1990: Models for Exceedances over High Thresholds. Journal of the Royal Statistical Society. Series B (Methodological), 52, 393-442.

de Haan, L., and A. Ferreira, 2007: Extreme value theory: an introduction. Springer Science & Business Media.

Dupuis, D. J., 1999: Exceedances over High Thresholds: A Guide to Threshold Selection. Extremes, 1, 251-261.

Gates, W. L., 1992: AMIP: The Atmospheric Model Intercomparison Project. Bulletin of the American Meteorological Society, 73, 1962-1970.

Goddard, L., and M. Dilley, 2005: El Niño: Catastrophe or Opportunity. Journal of Climate, 18, 651-665.

Guilyardi, E., and Coauthors, 2009: Understanding El Niño in Ocean–Atmosphere General Circulation Models: Progress and Challenges. Bulletin of the American Meteorological Society, 90, 325-340.

Hastenrath, S., L. Greischar, and J. van Heerden, 1995: Prediction of the Summer Rainfall over South Africa. Journal of Climate, 8, 1511-1518.

Hoell, A., C. Funk, T. Magadzire, J. Zinke, and G. Husak, 2015: El Niño–Southern Oscillation diversity and Southern Africa teleconnections during Austral Summer. Clim Dyn, 45, 1583-1599.

Hoell, A., C. Funk, J. Zinke, and L. Harrison, 2016: Modulation of the Southern Africa precipitation response to the El Niño Southern Oscillation by the subtropical Indian Ocean Dipole. Clim Dyn, 1-12.

Hurrell, J. W., J. J. Hack, D. Shea, J. M. Caron, and J. Rosinski, 2008: A New Sea Surface Temperature and Sea Ice Boundary Dataset for the Community Atmosphere Model. Journal of Climate, 21, 5145-5153.

IFRC, cited 2017: Southern Africa floods. [Available online at http://www.ifrc.org/southern-africa-floods.]

Jury, M. R., 2013: Variability in the Tropical Southwest Indian Ocean and Influence on Southern Africa Climate. International Journal of Marine Science, 3, 46-64.

Jury, M. R., C. Mc Queen, and K. Levey, 1994: SOI and QBO signals in the African region. Theor Appl Climatol, 50, 103-115.

Kalnay, E., and Coauthors, 1996: The NCEP/NCAR 40-Year Reanalysis Project. Bulletin of the American Meteorological Society, 77, 437-471.

Kuhnel, I., 1989: Tropical-extratropical cloudband climatology based on satellite data. International Journal of Climatology, 9, 441-463.

Landman, W. A., and L. Goddard, 2005: Predicting southern African summer rainfall using a combination of MOS and perfect prognosis. Geophysical Research Letters, 32, n/a-n/a.

Lindesay, J. A., 1988: South African rainfall, the Southern Oscillation and a Southern Hemisphere semi-annual cycle. Journal of Climatology, 8, 17-30.

Lyon, B., and S. J. Mason, 2009: The 1997/98 Summer Rainfall Season in Southern Africa. Part II: Model Simulations and Coupled Model Forecasts. Journal of Climate, 22, 3802-3818.

Manatsa, D., C. H. Matarira, and G. Mukwada, 2011: Relative impacts of ENSO and Indian Ocean dipole/zonal mode on east SADC rainfall. International Journal of Climatology, 31, 558-577.

Manatsa, D., T. Mushore, and A. Lenouo, 2015: Improved predictability of droughts over southern Africa using the standardized precipitation evapotranspiration index and ENSO. Theor Appl Climatol, 1-16.

Manatsa, D., C. J. C. Reason, and G. Mukwada, 2012: On the decoupling of the IODZM from southern Africa Summer rainfall variability. International Journal of Climatology, 32, 727-746.

Mason, S. J., and M. R. Jury, 1997: Climatic variability and change over southern Africa: a reflection on underlying processes. Progress in Physical Geography, 21, 23-50.

Misra, V., 2003: The Influence of Pacific SST Variability on the Precipitation over Southern Africa. Journal of Climate, 16, 2408-2418.

Nicholson, S., and D. Entekhabi, 1986: The quasi-periodic behavior of rainfall variability in Africa and its relationship to the southern oscillation. Arch. Met. Geoph. Biocl. A., 34, 311-348.

Nicholson, S. E., and J. Kim, 1997: THE RELATIONSHIP OF THE EL NIÑO–SOUTHERN OSCILLATION TO AFRICAN RAINFALL. International Journal of Climatology, 17, 117-135.

Parent, E., and J. Bernier, 2003: Bayesian POT modeling for historical data. Journal of Hydrology, 274, 95-108.

Ratnam, J. V., S. K. Behera, Y. Masumoto, and T. Yamagata, 2014: Remote Effects of El Niño and Modoki Events on the Austral Summer Precipitation of Southern Africa. Journal of Climate, 27, 3802-3815.

Reason, C. J. C., 1998: Warm and cold events in the southeast Atlantic/southwest Indian Ocean region and potential impacts on circulation and rainfall over southern Africa. Meteorol. Atmos. Phys., 69, 49-65.

——, 1999: Interannual warm and cool events in the subtropical/mid-latitude South Indian Ocean Region. Geophysical Research Letters, 26, 215-218.

——, 2001: Subtropical Indian Ocean SST dipole events and southern African rainfall. Geophysical Research Letters, 28, 2225-2227.

Reason, C. J. C., R. J. Allan, J. A. Lindesay, and T. J. Ansell, 2000: ENSO and climatic signals across the Indian Ocean Basin in the global context: part I, interannual composite patterns. International Journal of Climatology, 20, 1285-1327.

Reason, C. J. C., and D. Jagadheesha, 2005: A model investigation of recent ENSO impacts over southern Africa. Meteorol. Atmos. Phys., 89, 181-205.

Reason, C. J. C., and H. Mulenga, 1999: Relationships between South African rainfall and SST anomalies in the Southwest Indian Ocean. International Journal of Climatology, 19, 1651-1673.

——, 1999: Relationships between South African rainfall and SST anomalies in the Southwest Indian Ocean. International Journal of Climatology, 19, 1651-1673.

Rocha, A., and I. A. N. Simmonds, 1997: INTERANNUAL VARIABILITY OF SOUTH-EASTERN AFRICAN SUMMER RAINFALL. PART 1: RELATIONSHIPS WITH AIR–SEA INTERACTION PROCESSES. International Journal of Climatology, 17, 235-265.

Roeckner, E., and Coauthors, 2006: Sensitivity of Simulated Climate to Horizontal and Vertical Resolution in the ECHAM5 Atmosphere Model. Journal of Climate, 19, 3771-3791.

Ropelewski, C. F., and M. S. Halpert, 1987: Global and Regional Scale Precipitation Patterns Associated with the El Niño/Southern Oscillation. Monthly Weather Review, 115, 1606-1626.

Rouault, M., P. Florenchie, N. Fauchereau, and C. J. C. Reason, 2003: South East tropical Atlantic warm events and southern African rainfall. Geophysical Research Letters, 30, n/a-n/a.

Saha, S., and Coauthors, 2013: The NCEP Climate Forecast System Version 2. Journal of Climate, 27, 2185-2208.

Schneider, U., A. Becker, P. Finger, A. Meyer-Christoffer, M. Ziese, and B. Rudolf, 2013: GPCC's new land surface precipitation climatology based on quality-controlled in situ data and its role in quantifying the global water cycle. Theor Appl Climatol, 115, 15-40.

Todd, M., and R. Washington, 1999: Circulation anomalies associated with tropical-temperate troughs in southern Africa and the south west Indian Ocean. Clim Dyn, 15, 937-951.

Vidal, J., 2016: Southern Africa cries for help as El Niño and climate change savage maize harvest. The Guardian.

Wang, B., and Coauthors, 2009: Advance and prospectus of seasonal prediction: assessment of the APCC/CliPAS 14-model ensemble retrospective seasonal prediction (1980–2004). Clim Dyn, 33, 93-117.

Wang, F., 2010: Subtropical dipole mode in the Southern Hemisphere: A global view. Geophysical Research Letters, 37, n/a-n/a.

Washington, R., and A. Preston, 2006: Extreme wet years over southern Africa: Role of Indian Ocean sea surface temperatures. Journal of Geophysical Research: Atmospheres, 111, n/a-n/a.

Wyrtki, K., 1975: El Niño—The Dynamic Response of the Equatorial Pacific Oceanto Atmospheric Forcing. Journal of Physical Oceanography, 5, 572-584.

Yang, C., and B. S. Giese, 2013: El Niño Southern Oscillation in an ensemble ocean reanalysis and coupled climate models. Journal of Geophysical Research: Oceans, 118, 4052-4071.

Yuan, C., T. Tozuka, W. Landman, and T. Yamagata, 2014: Dynamical seasonal prediction of Southern African summer precipitation. Clim Dyn, 42, 3357-3374.

List of Tables

Table 1: December-March 1979-2016 ENSO and SIOD occurrences.

	ENSO Neutral	EN-SIOD	EN+SIOD	LN+SIOD	LN-SIOD
Season	1979-1980 1980-1981 1981-1982 1989-1990 1990-1991 1992-1993 1993-1994 1996-1997 2001-2002 2003-2004 2012-2013 2013-2014	1982-1983 1991-1992 1994-1995 1997-1998 2002-2003 2009-2010 2014-2015 2015-2016	1986-1987 1987-1988 2004-2005 2006-2007	1998-1999 2000-2001 2005-2006 2007-2008 2008-2009 2010-2011	1983-1984 1984-1985 1985-1986 1988-1989 1995-1996 1999-2000 2011-2012

Table 2: December-March standardized anomaly and standard deviation of areally averaged Southern Africa precipitation in AMIP simulations during ENSO occurrences.

	ENSO Neutral	EN+SIOD	EN-SIOD	LN+SIOD	LN-SIOD
Standardized Anomaly	-0.02	-0.17	-0.13	0.20	0.13
Standard Deviation	0.48	0.45	0.44	0.57	0.56

List of Figures

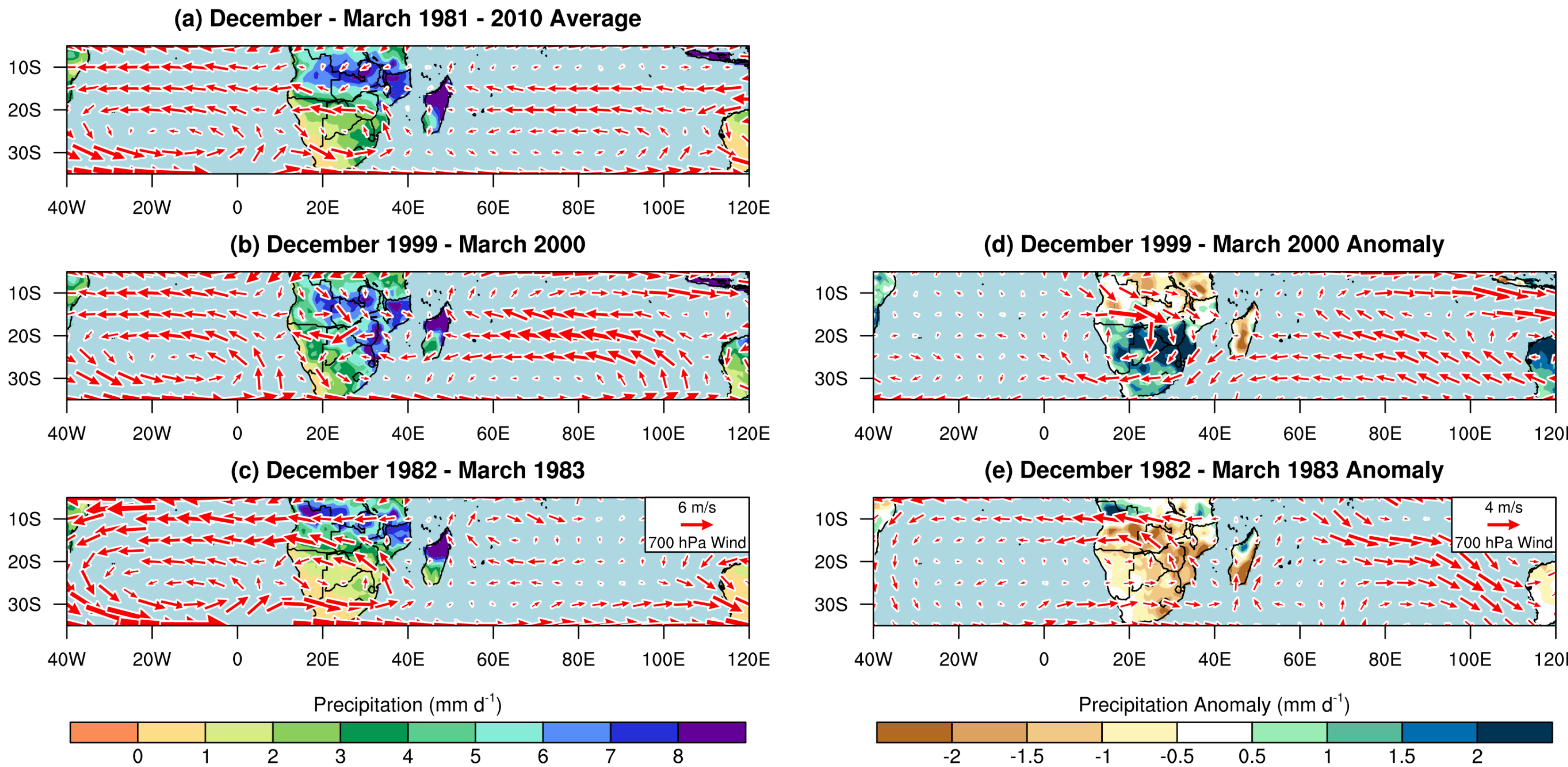

Figure 1: December-March GPCC precipitation (shading) and 700 hPa NCEP-NCAR Reanalysis 1 wind (vector) in terms of the (a) 1981-2010 30-yr average, (b) 1999-2000 season, (c) 1982-1983 season, (d) 1999-2000 seasonal anomaly and (e) 1982-1983 seasonal anomaly. 1999-2000 and 1982-1983 were the wettest and driest areally averaged Southern Africa precipitation seasons south of 15˚S, respectively, during 1979-2016.

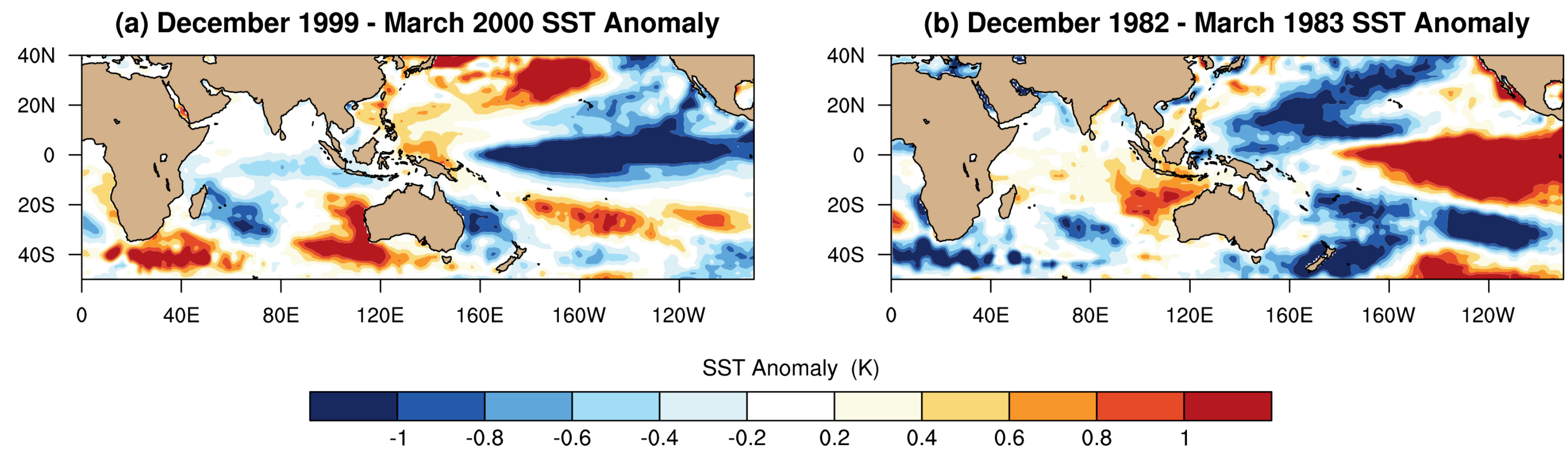

Figure 2: December-March Hurrell et al. (2008) SST anomaly during the (a) 1999-2000 and (b) 1982-1983 seasons.

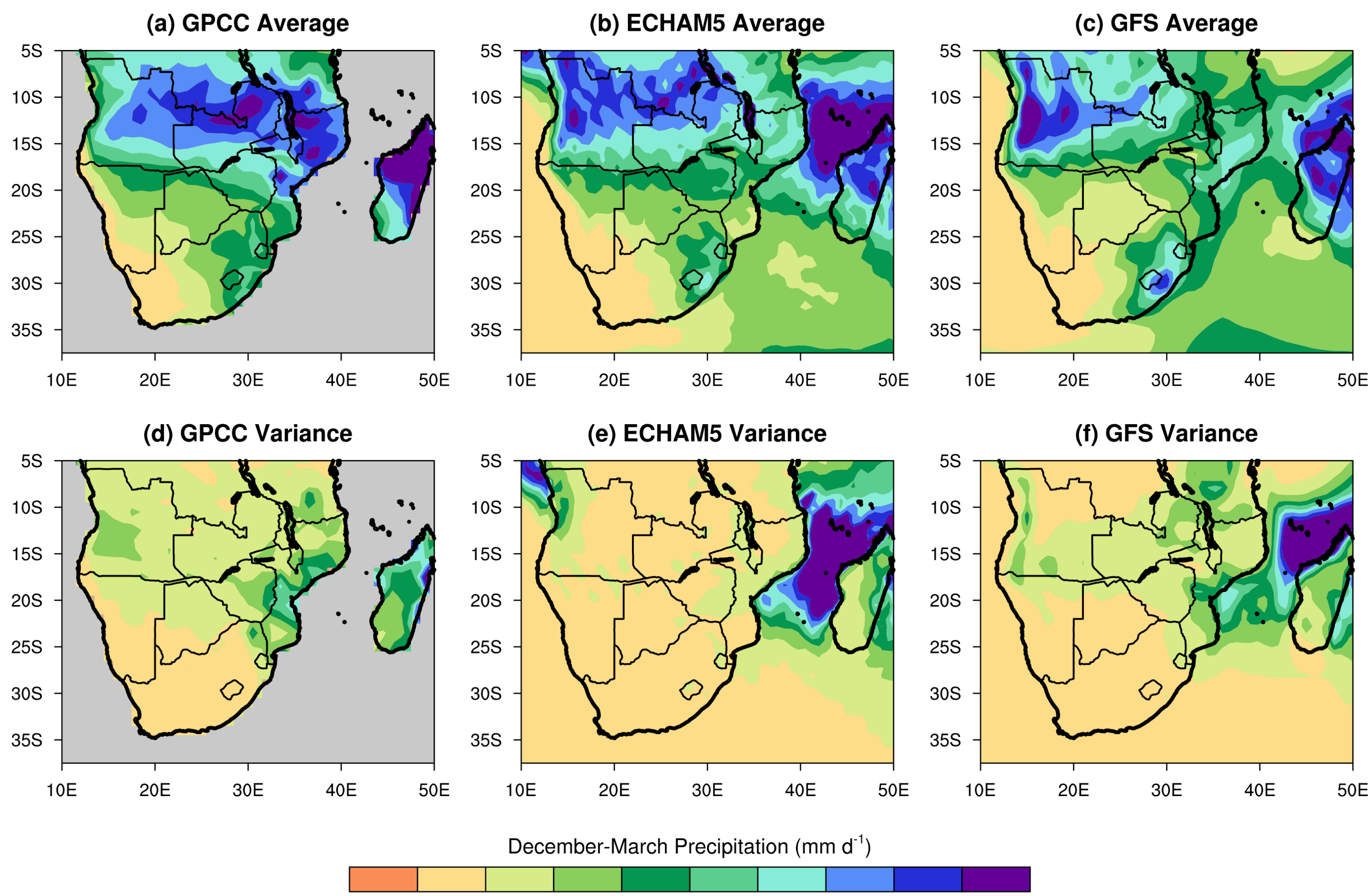

Figure 3: December-March 1979-2016 (top row) average precipitation (mm d^{-1}) and (bottom row) precipitation variance (mm d^{-1}) resolved by (left column) GPCC, (center column) ECHAM5 AMIP simulations and (right column) GFS AMIP simulations.

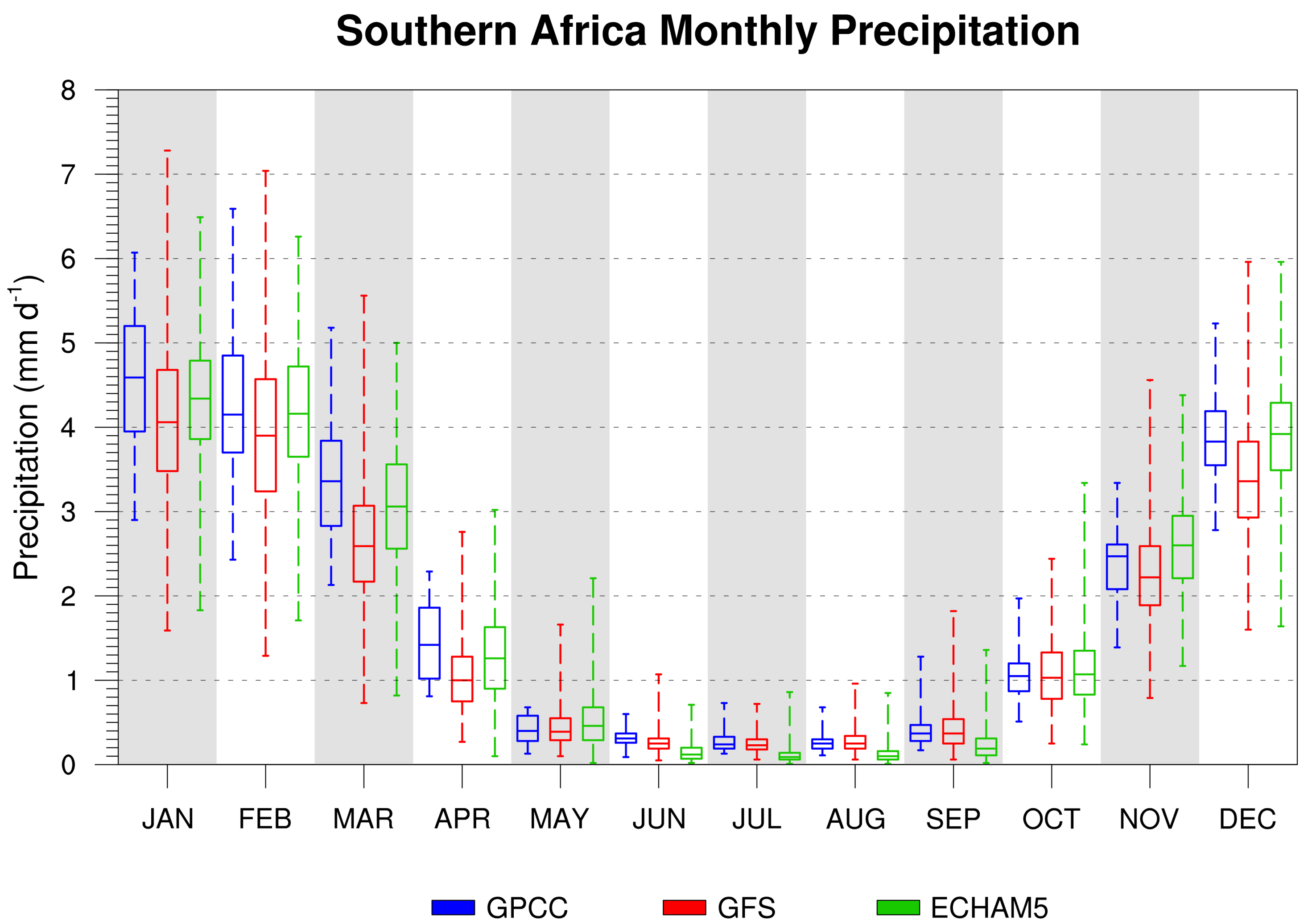

Figure 4: Box and whisker plot of monthly 1979-2016 Southern Africa precipitation (mm d^{-1}) for GPCC (blue), GFS AMIP simulations (red) and ECHAM5 AMIP simulations (green).

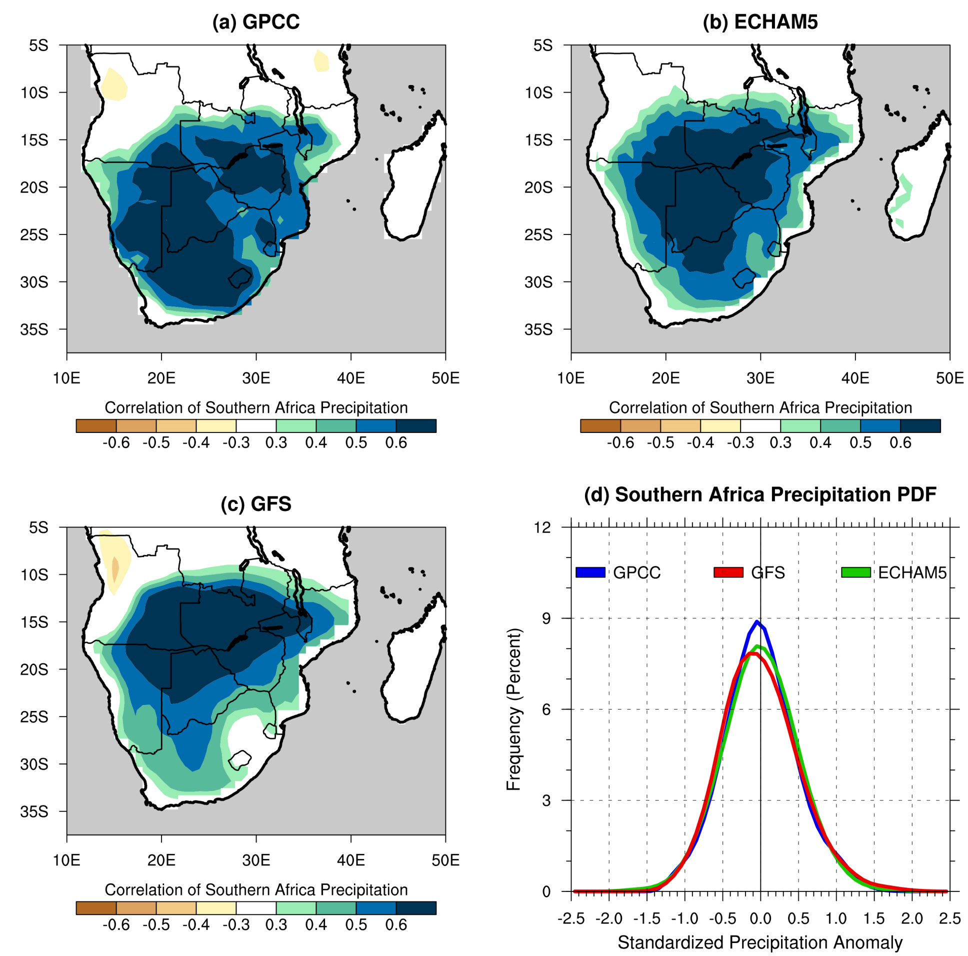

Figure 5: December-March 1979-2016 correlation of areally averaged Southern Africa precipitation anomaly with the spatial precipitation anomaly for (a) GPCC, (b) ECHAM5 AMIP simulations and (c) GFS AMIP simulations. (d) December-March 1979-2016 areally averaged Southern Africa standardized precipitation anomaly PDFs for GPCC (blue), ECHAM5 AMIP simulations (green) and GFS AMIP simulations (red).

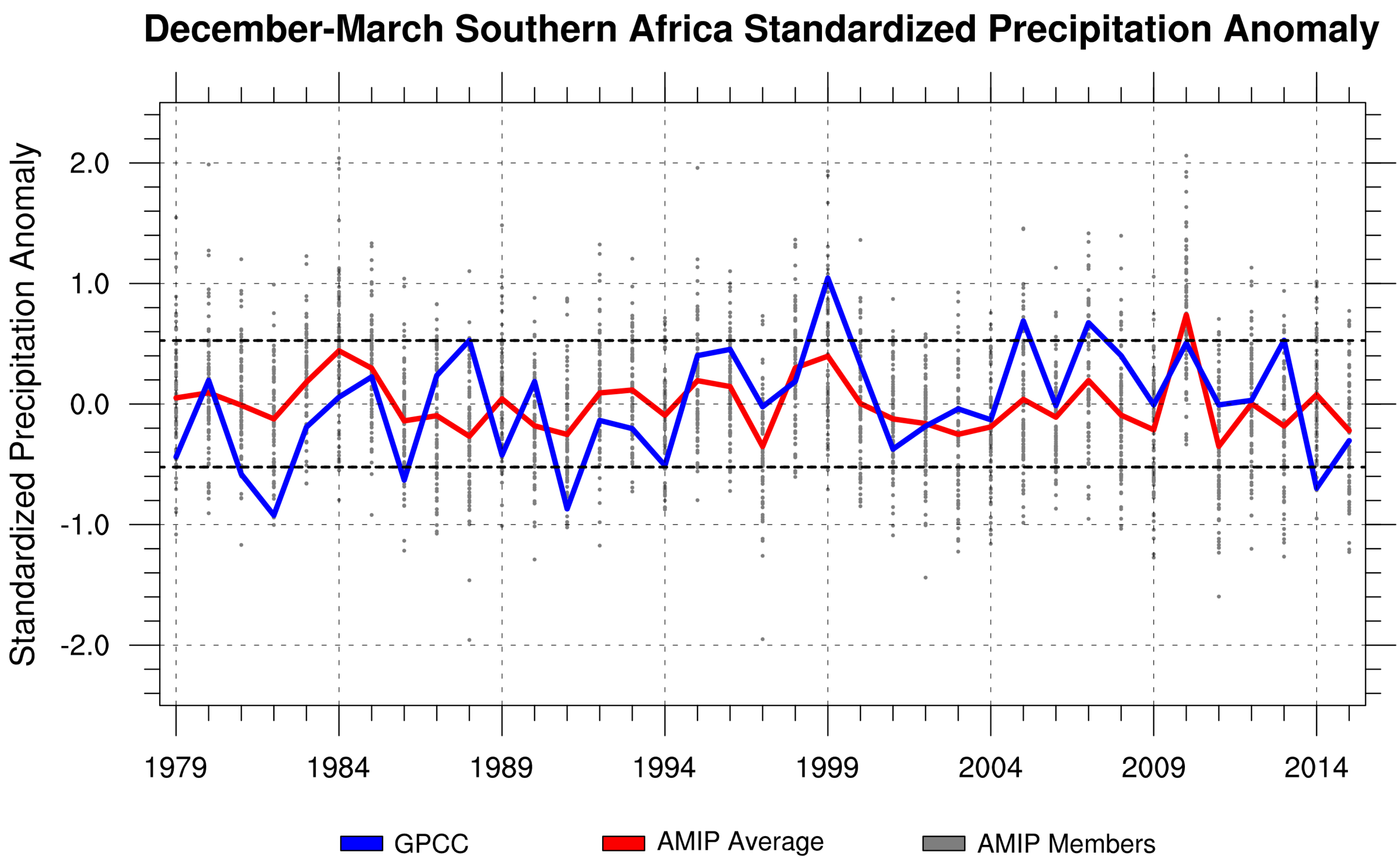

Figure 6: December-March 1979-2016 areally averaged Southern Africa standardized precipitation anomaly displayed in terms of ensemble members of AMIP simulations (gray dots), the ensemble average of AMIP simulations (red line) and GPCC (blue line). The horizontal solid dashed lines denote extremes at the 15% (dry) and 85% (wet) quantiles for the ensemble members of AMIP simulations. Labeled years on the ordinate correspond with December.

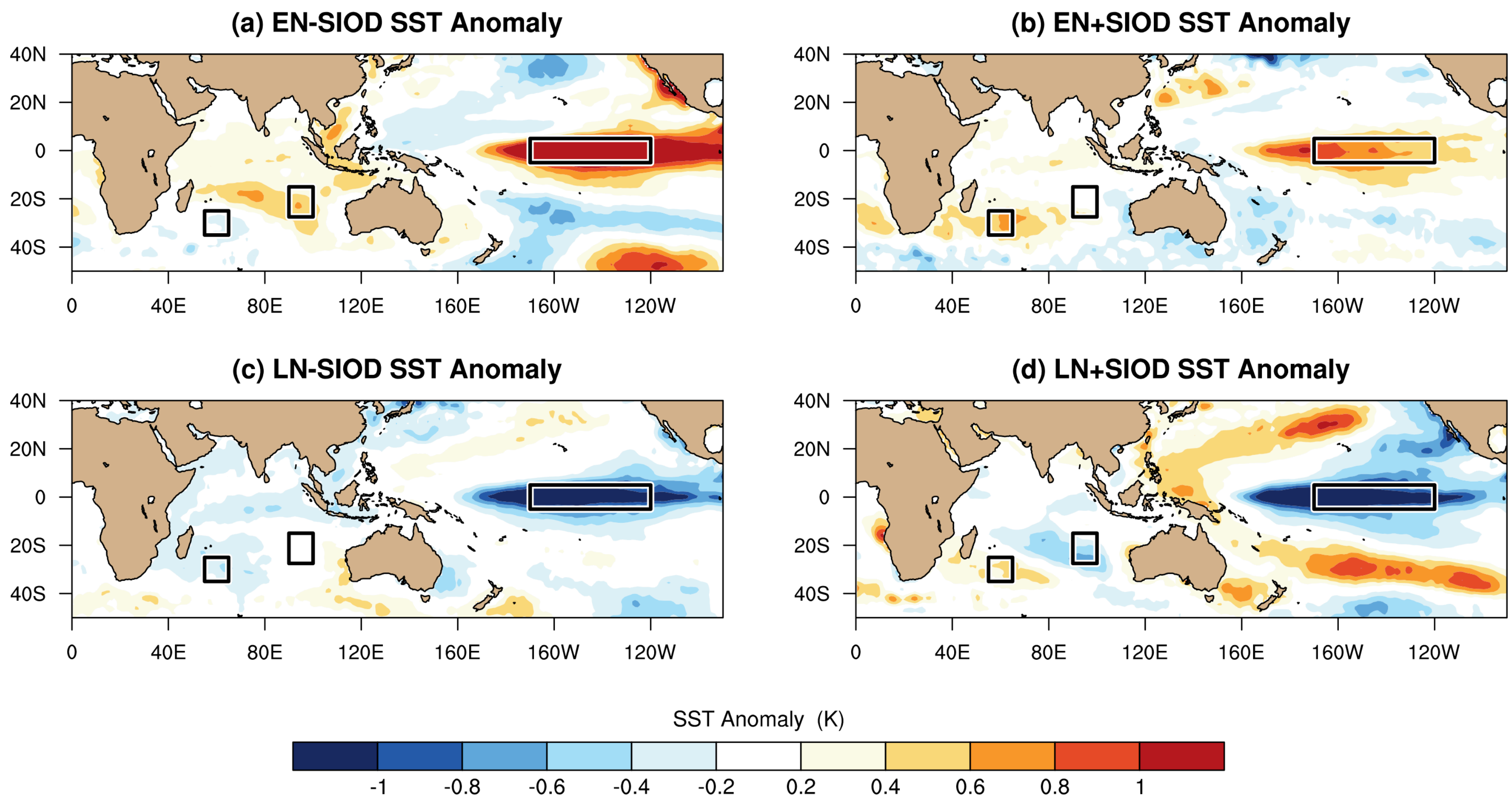

Figure 7: December-March 1979-2016 average SST anomaly (K) during (a) EN-SIOD, (b) EN+SIOD, (c) LN-SIOD and (d) LN+SIOD. The Niño3.4 region and the regions that define the SIOD are plotted in black.

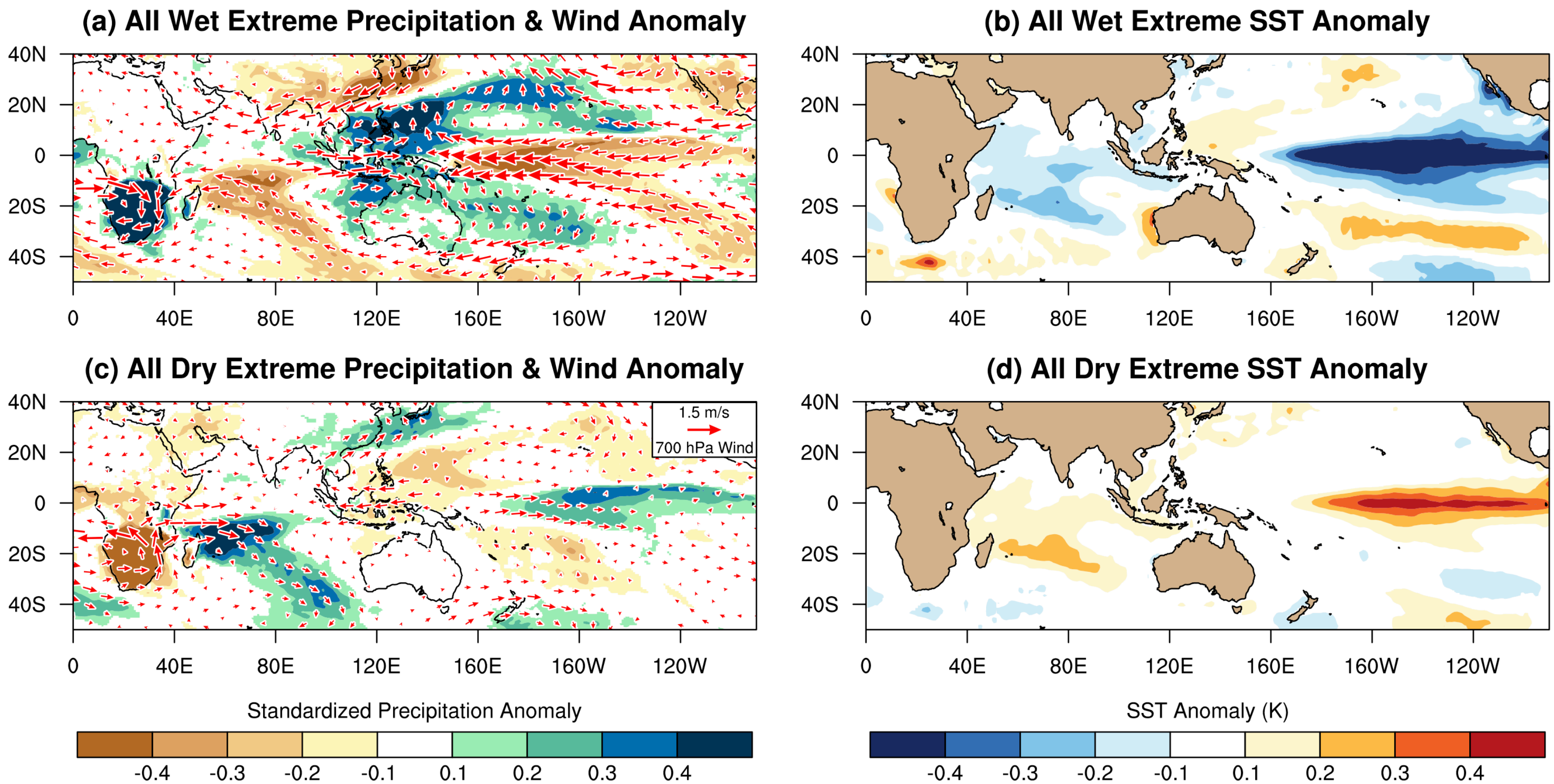

Figure 8: December-March averages of (left column) AMIP simulated standardized precipitation anomaly (shading) and 700 hPa wind anomaly (vectors; m s^{-1}) and (right column) SST anomaly (K) during (top row) extreme wet and (bottom row) extreme dry Southern Africa precipitation seasons. All displayed variables are significant at p<0.05.

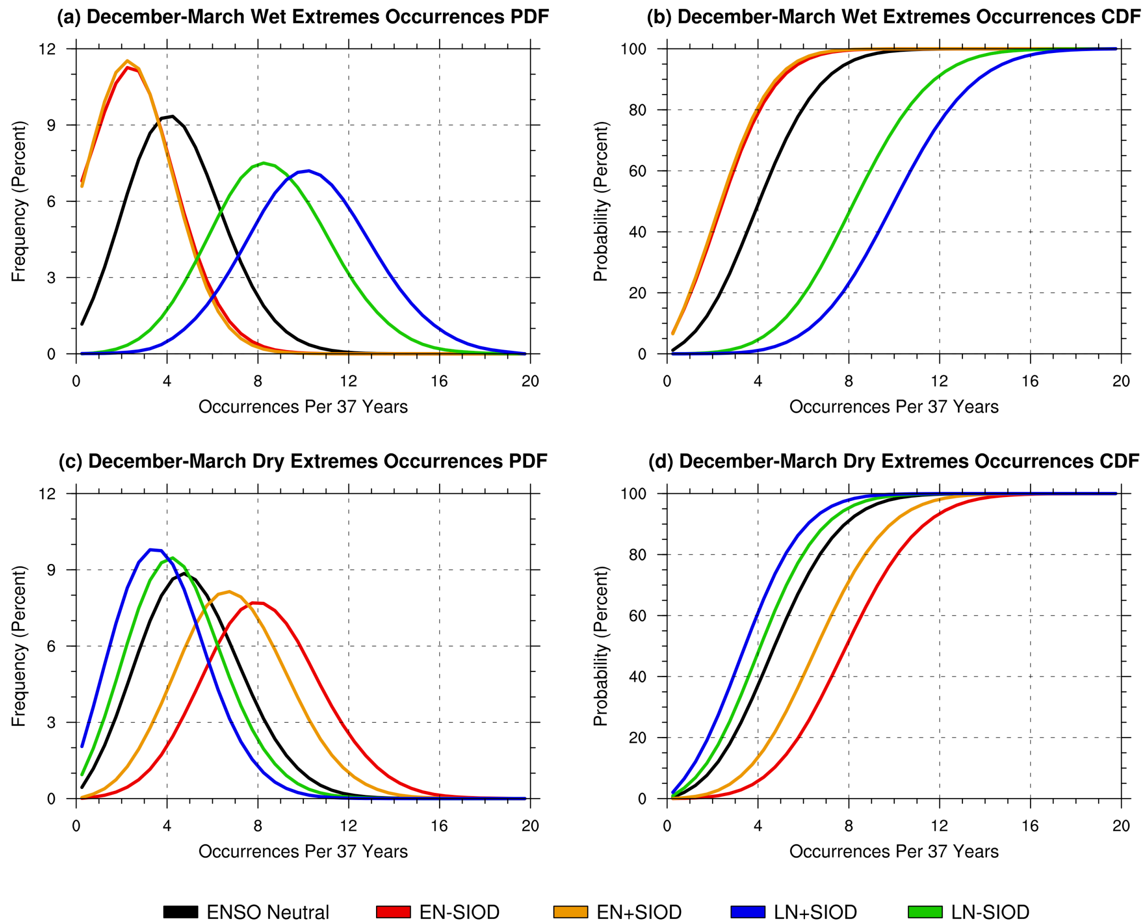

Figure 9: Distributions of December-March 1979-2016 Southern Africa (top row) wet and (bottom row) dry extremes during ENSO and SIOD phase combinations in terms of (left column) probability distribution functions and (right column) cumulative distribution functions in AMIP simulations.

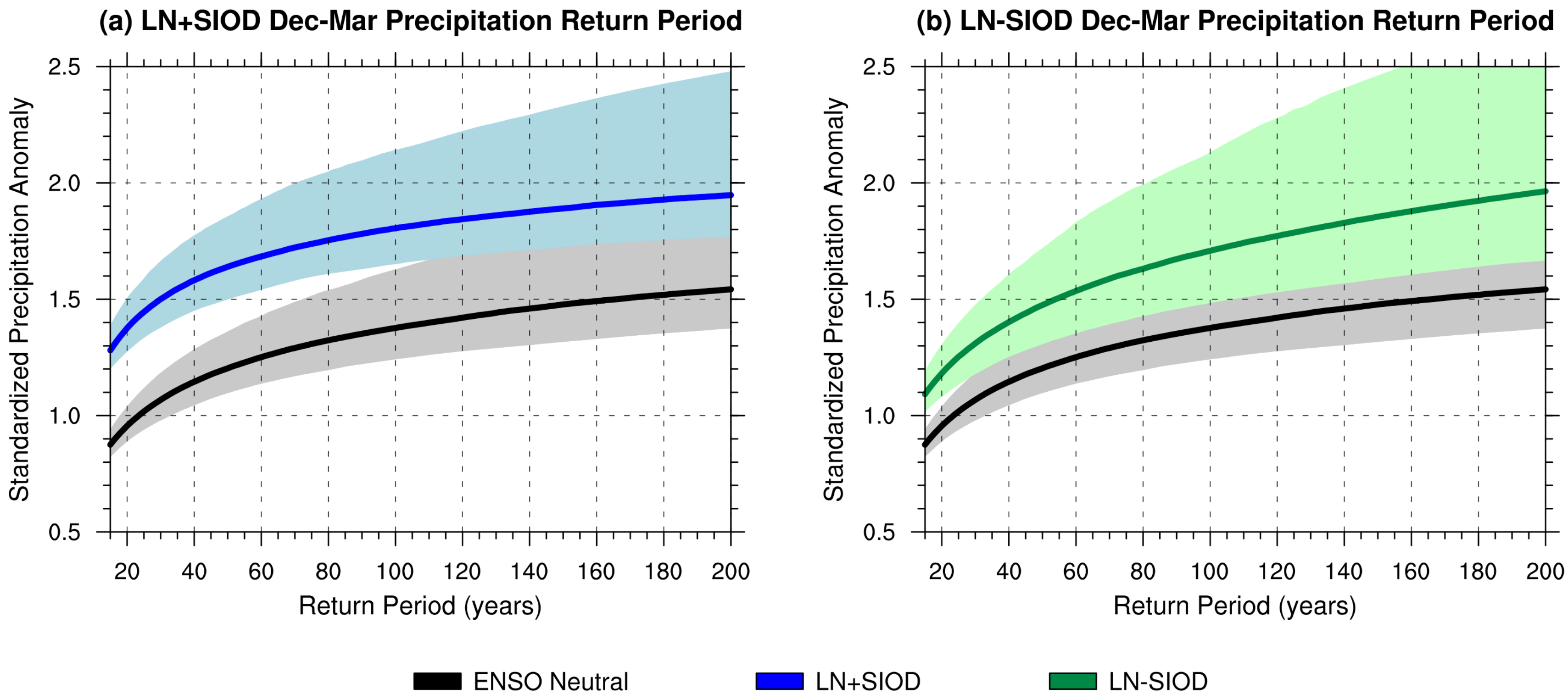

Figure 10: Estimations of return level (standardized anomaly) and return period (years) based on exceedances above the 85% quantile of standardized rainfall displayed in terms of the median (solid line) and the 95th percentiles (shading) for (a) LN+SIOD and ENSO Neutral and (b) LN-SIOD and ENSO neutral.

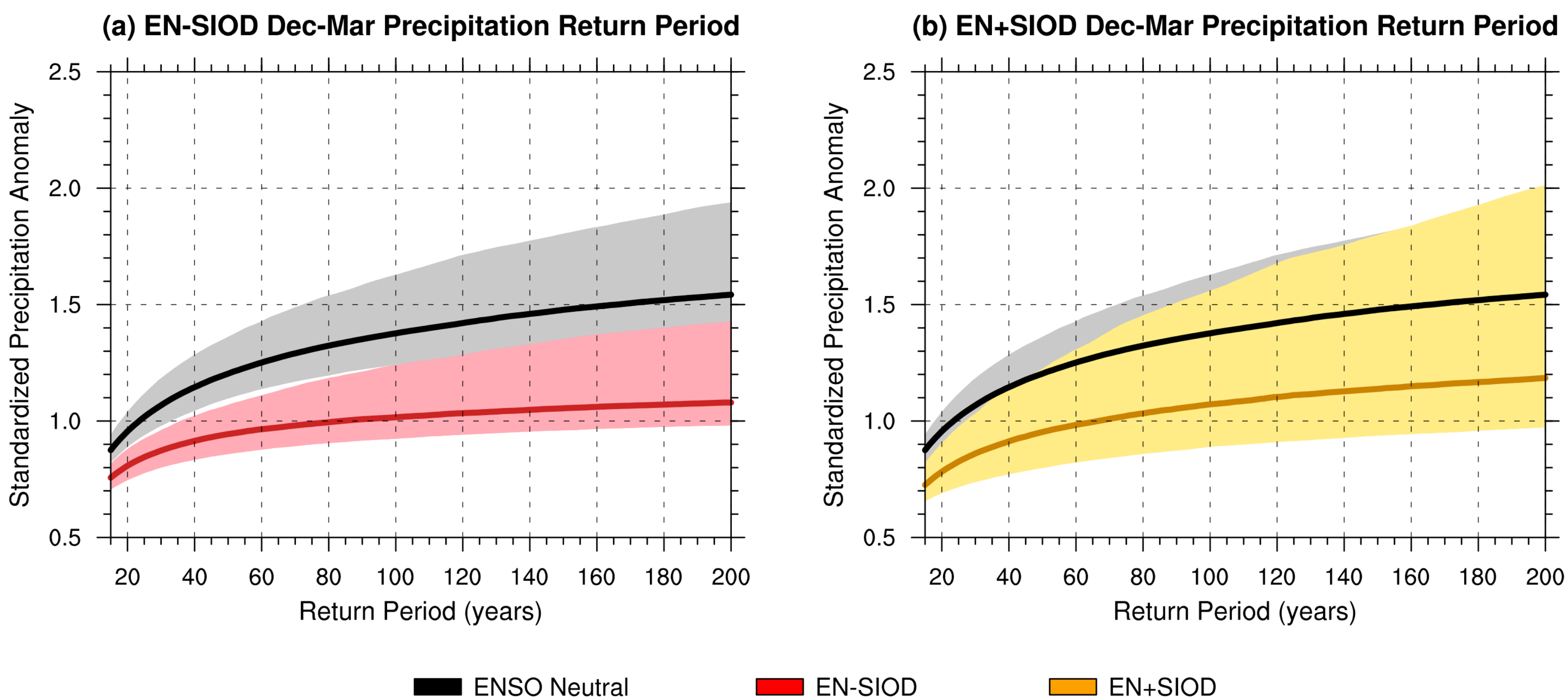

Figure 11: Estimations of return level (standardized anomaly) and return period (years) based on exceedances above the 85% quantile of standardized rainfall displayed in terms of the median (solid line) and the 95th percentiles (shading) for (a) EN-SIOD and ENSO neutral and (b) EN+SIOD and ENSO Neutral.

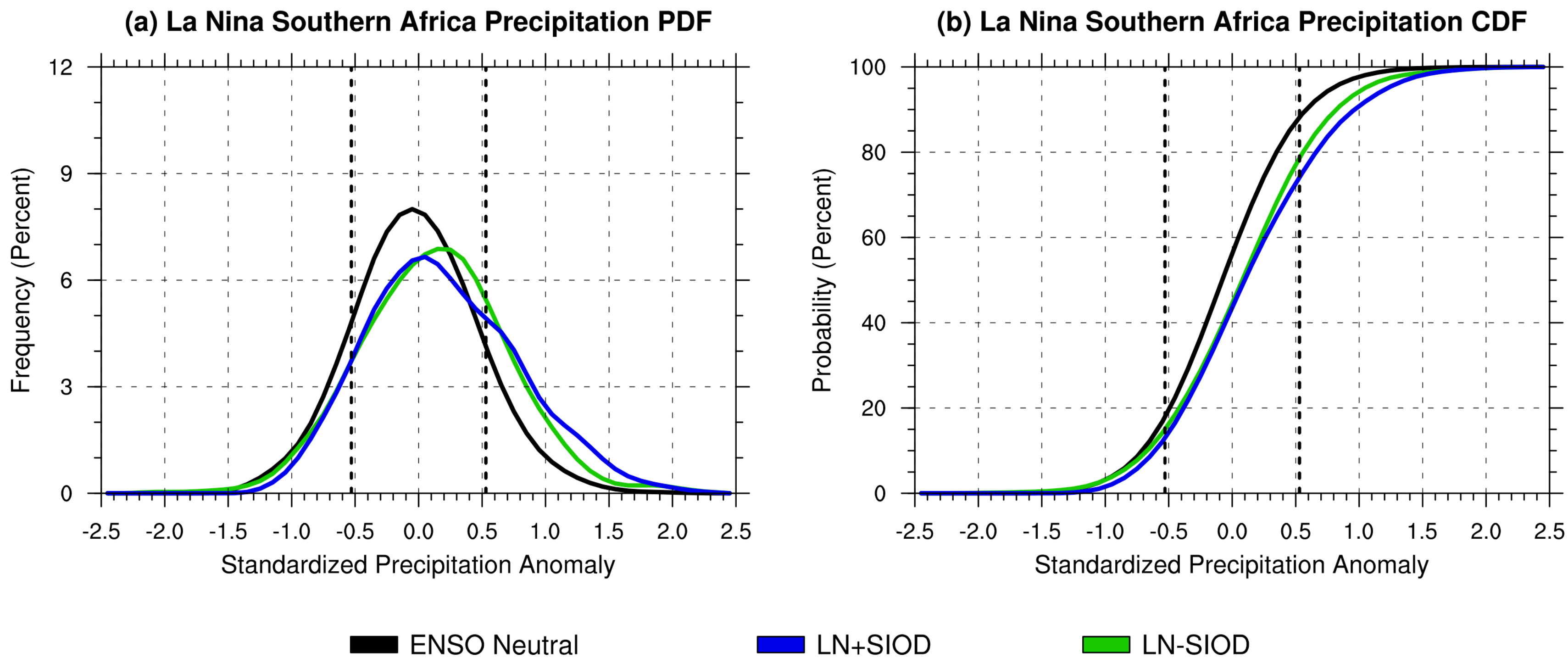

Figure 12: December-March 1979-2016 areally averaged Southern Africa standardized precipitation anomaly in AMIP simulations during ENSO neutral (black line), LN+SIOD (blue line) and LN-SIOD (green line) displayed in terms of (a) probability distribution functions and (b) cumulative distribution functions. The solid dashed lines denote extremes at the 15% (dry) and 85% (wet) quantiles for all of the AMIP ensemble members (same as in Fig. 5).

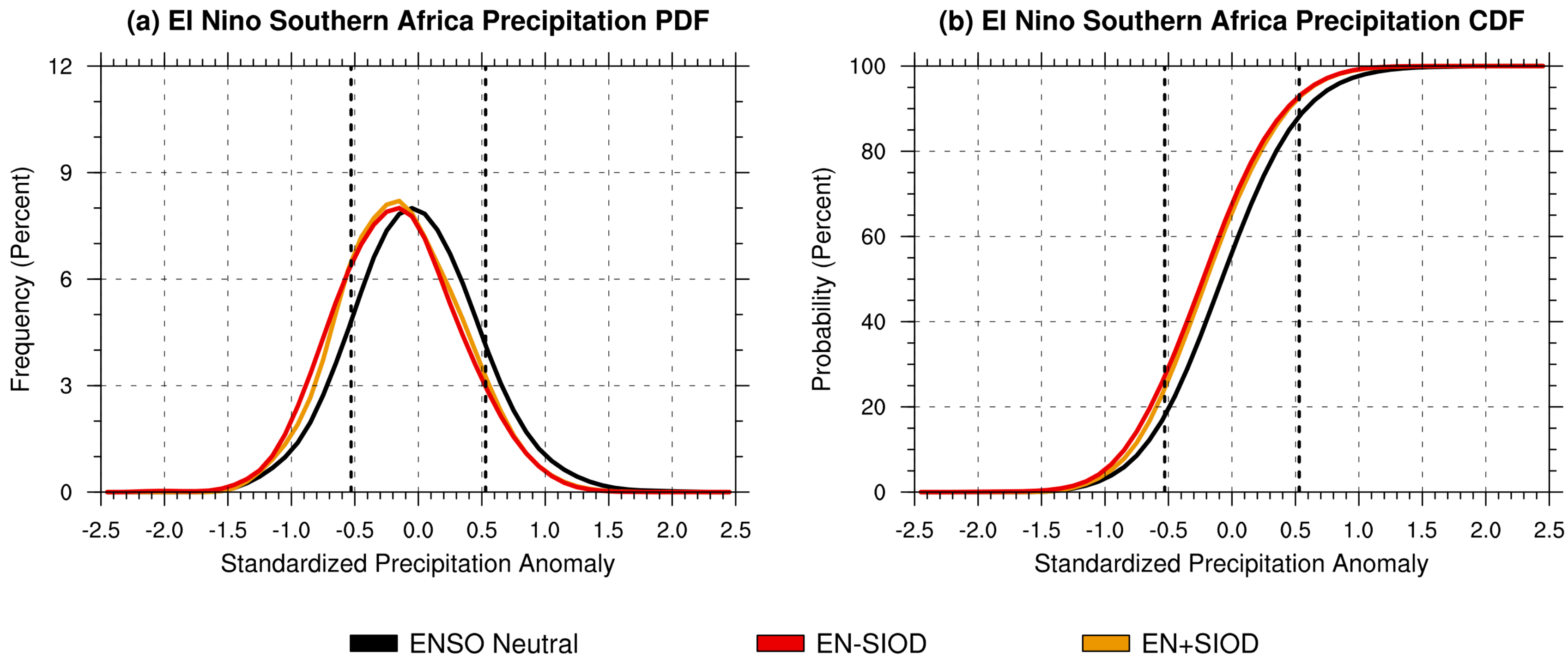

Figure 13: December-March 1979-2016 areally averaged Southern Africa standardized precipitation anomaly in AMIP simulations during ENSO neutral (black line), EN-SIOD (red line) and EN+SIOD (orange line) displayed in terms of (a) probability distribution functions and (b) cumulative distribution functions. The solid dashed lines denote extremes at the 15% (dry) and 85% (wet) quantiles for all of the AMIP ensemble members (same as in Fig. 5).

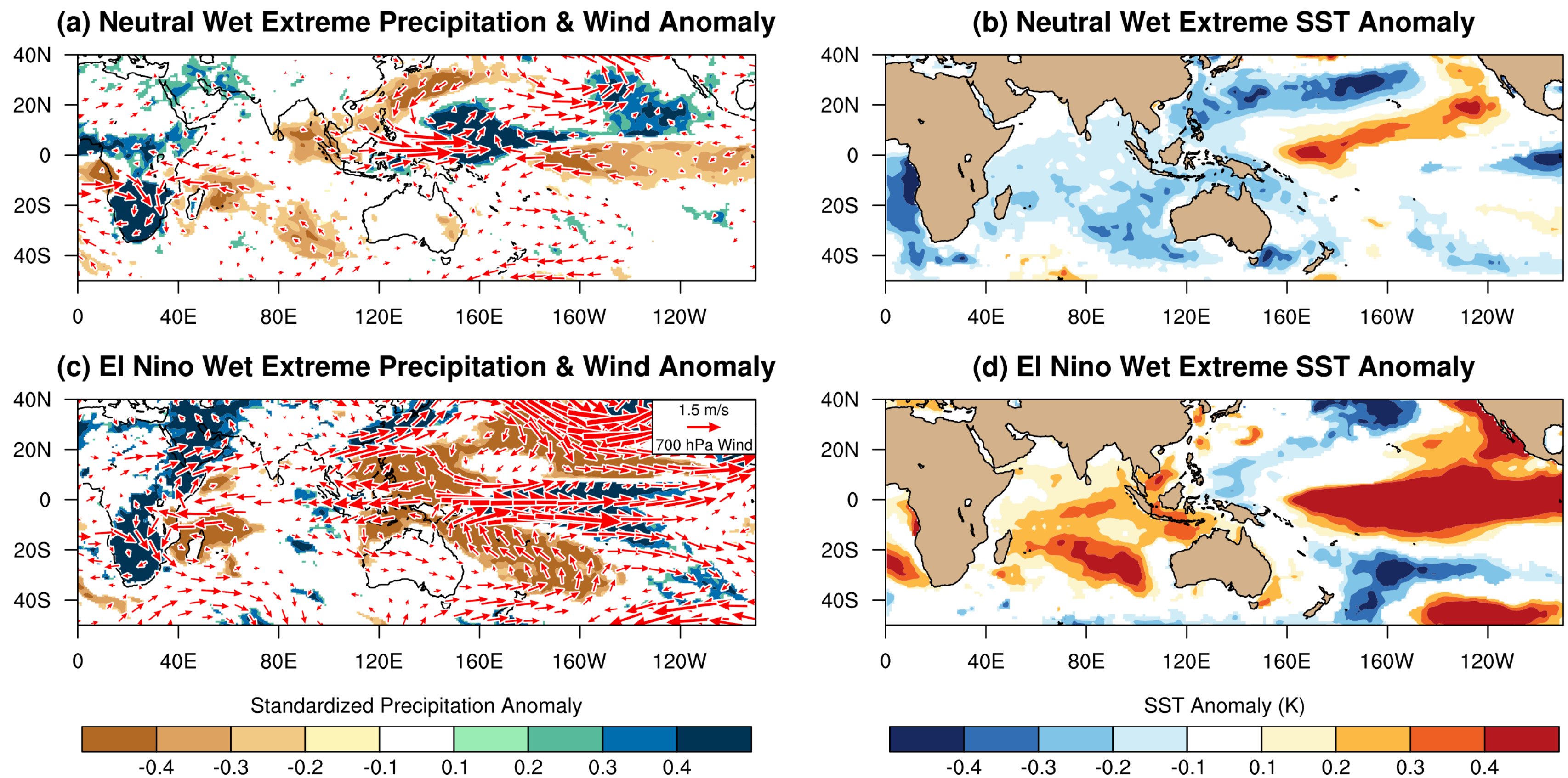

Figure 14: December-March averages of (left column) AMIP simulated standardized precipitation anomaly (shading) and 700 hPa wind anomaly (vectors; m s^{-1}) and (right column) SST anomaly (K) during extreme Southern Africa wet seasons during (top row) ENSO neutral and (bottom row) El Niño. All displayed variables are significant at $p<0.05$.

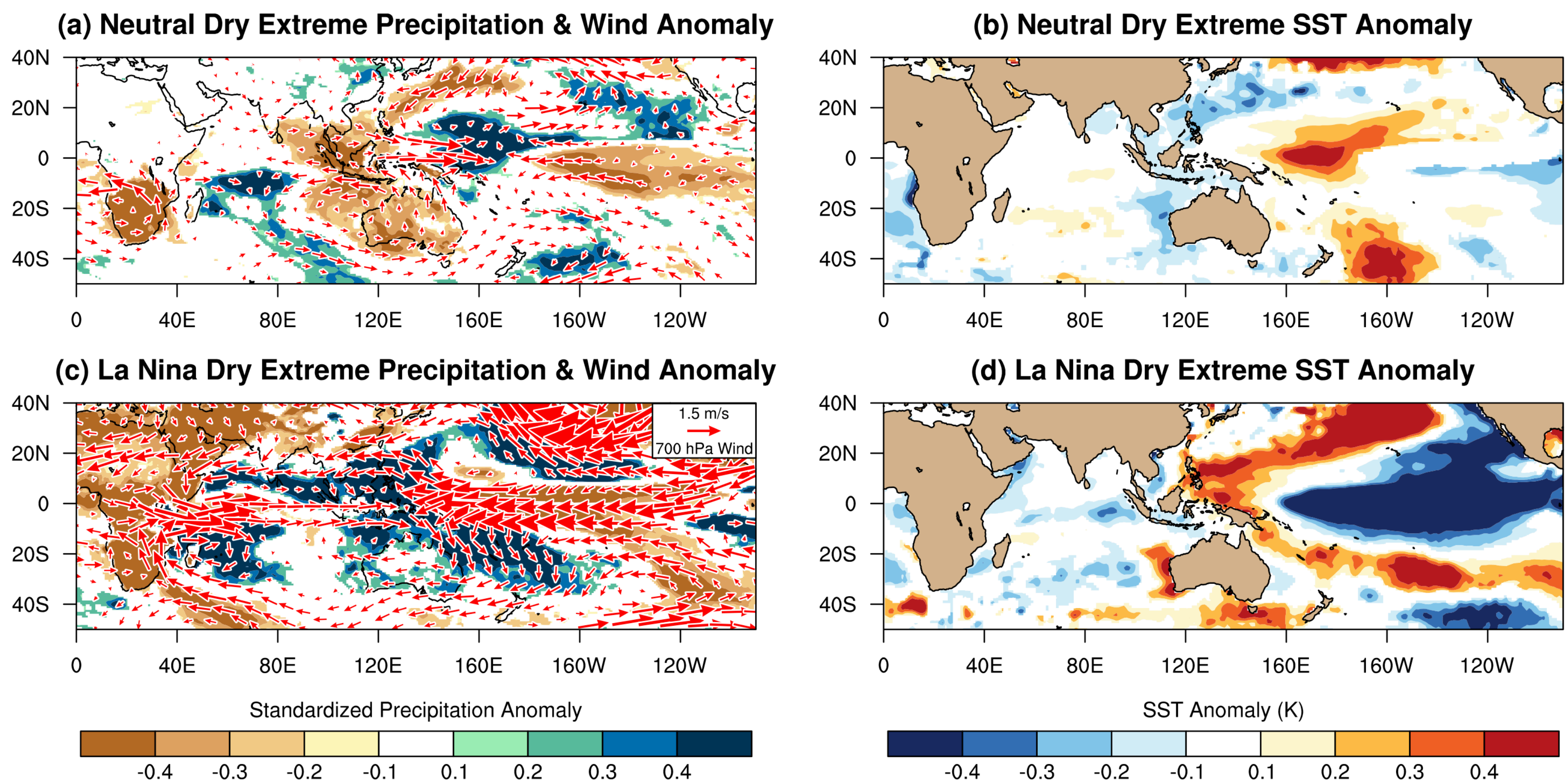

Figure 15: December-March averages of (left column) AMIP simulated standardized precipitation anomaly (shading) and 700 hPa wind anomaly (vectors; m s^{-1}) and (right column) SST anomaly (K) during extreme Southern Africa dry seasons during (top row) ENSO neutral and (bottom row) La Niña. All displayed variables are significant at p<0.05.